Second Annual Progress Report
NASW-5036
Penetration electric fields and inner magnetosphere dynamics - A model and data comparison

Nelson C. Maynard, PI
Mission Research Corporation
Nashua, New Hampshire

27 February 1998

Covering period from 6 March 1997 through 5 March 1998

Second Annual Progress Report
NASW-5036
6 March 1997 through 5 March 1998

Scientific highlights from the June 1991 storm:

- All particle and field boundaries move equatorward during the initial phase of the storm
- Electric field boundaries were close to the inner edge of the ring current or at lower L shells throughout the main and recovery phases
- Electric potentials at subauroral latitudes were large fractions of the total potentials in the afternoon cell
- The equatorward boundary of auroral electron precipitation mirrored the electric field boundary, but showed a higher degree of variability, partially from inflation from the storm-time ring current

Summary:

Significant progress has been made on the analysis of the June, 1991 storm. We have completed the analysis of the CRRES and DMSP data sets. We have been able to follow the evolution during the storm of the inner edge of the electric field patterns in the dusk sector and its relation to electron boundaries, ion boundaries and the ring current. Whereas the CRRES data provide radial cuts out through the plasmasphere every 10 hours, DMSP provides snapshots every orbit of the potential and particle boundaries. Electric field and energetic particle measurements from CRRES and ion drifts and energetic particle measurements from DMSP provide the principal data sets. The combined data set provides high resolution definition of the boundary motions over the phases of the storm. L shell differences between the DMSP and CRRES particle boundaries are easily explained by inflation of the dusk sector by the ring current. The electric field boundaries are typically associated with the ion boundary and the inner edge of the ring current except during rapid increases in the cross-polar cap potential. A significant fraction of the dusk cell potential is found inside the plasmasheet electron inner edge. Twice during the storm this potential exceeded 60 kV. A paper (copy attached) has been prepared (Burke et al., 1998) and submitted to JGR. An invited paper will be presented by Burke at the spring AGU meeting. An abstract has also been submitted to the COSPAR meeting for presentation by Maynard.

New simulations have been carried out with the Rice Convection Model for the magnetic storm of June 4-5, 1991, and comparisons have been made with CRRES and DMSP data. These RCM runs contained several major code improvements:

1. The magnetic fields vary continuously through the event, using input magnetic field models scaled with standoff distance, Dst, and auroral boundary index; this allows study of the subtle effects of large-scale changes in magnetospheric configuration on ring-current injection.
2. The high-L boundary of the RCM calculation varies continuously in time and is not aligned with a grid line.
3. The initial condition includes a representation of the quiet-time ring current. This allows us to evaluate how much of the storm-time ring current consists of fresh plasma from the plasma sheet and how much consists of pre-existing ring-current particles that have been energized in the storm and injected deeper into the magnetosphere.

Simulation results have been compared with CRRES observations. A detailed comparison has been carried out for one particularly interesting pass, the outbound part of orbit 766. The RCM predicts that electric fields at MLT = 17 peak near L = 4, in agreement with observations. Model and measurements are also in rough agreement with regard to peak strength, but the RCM predicts stronger electric fields at higher L than were actually observed by CRRES. RCM predictions were also compared with measurements of the time-dependent L-values of the duskside electron inner edge and electric-field boundary; agreement was good during the main phase of the storm, less impressive at the beginning of the event. A paper by Garner et al. was presented at the fall AGU meeting. An abstract by Garner et al. has been submitted to the spring AGU meeting.

Future directions:

Our study of the June 1991 magnetic storm will continue in several directions into the third year of the contract. We will continue our collaboration with Dick Wolf's group at Rice University to simulate the development of the ring current and its role in shielding electric fields from the innermost parts of the magnetosphere. Gussenhoven and Burke plan to study empirical relationships between auroral electron boundaries and penetration electric fields as a function of magnetic local time away from the dusk sector using measurements from all three DMSP satellites that were operating at the time of the storm.

We plan to continue the data analysis with the selection of another storm. Two candidates are being investigated. The August 1990 storm is complementary to the present study by providing data on the dawn side. In addition to understanding the elctrodynamics of the dawnside during storms, this event would provide insight for magnetic field modelers relative to ring currents and storm time effects. The second candidate is the July 1991 storm. This storm is when CRRES is obtaining data on the dusk side, similar to the June storm. It has a unique feature of a long, gradually decreasing period of negative IMF Bz during the period of maximum negative DST. We plan to proceed with the study of one or both of these storms. Howard Singer will help choose the first candidate to be analyzed and will assist in the determination of ring current effects based on the magnetic field data.

In the modeling ares, we plan further analysis of the June 1991 storm to investigate several fundamental issues with regard to the injection of the storm-time ring current:

1. Can our model calculations explain CRRES observations of very strong electric fields earthward of the duskside electron plasma sheet in large storms? The tentative answer, based on the initial set of RCM runs, seems to be "yes."
2. Does a significant fraction of the storm-time ring current result from acceleration of particles that were in the quiet-time ring current before the storm? This possibility was suggested years ago by Lyons and Williams but has never been systematically investigated with a computational model. Again, the tentative answer, based on the first set of runs, seems to be "yes," but more careful study is needed.
3. Observations indicate large increases in fluxes of 100-keV ions at $L \sim 3$ during strong magnetic storms. A key question is: can a theoretical model with self-consistently computed electric field explain the observed increases? Or does some other mechanism, outside the conventional picture, have to be at work? Earlier work by Margaret Chen and collaborators suggested that it may not be possible to explain the observed increases in terms of models based on the conventional picture.
4. Does our improved model predict realistic penetration of the electric field to the mid- and low-latitude ionosphere ($L < 2$)? The first runs predict unrealistically strong fields at low latitudes.
5. Do electric fields generated by thermospheric winds substantially affect ring-current injection?

The Rice group is using the June 4-5, 1991, event as a focus for a major theoretical study of the ring current. Processing of input data for the event and comparisons with CRRES data have been supported almost entirely by this contract Much of the overall theoretical effort, and the accompanying code development, have been supported by NASA grant NAG5-4267 and NSF grant ATM-9613824.

Augmentation:

The Principal Investigator is the US representative for IACG Campaign 2 on boundary layers. That committee has decided to meet in conjunction with the COSPAR meeting in Nagoya, Japan, in July, 1998. As a result of conversations with Dr. Zannetti at NASA Headquarters, a cost proposal for that trip is attached for $4,540.00 as an augmentation to the funding for Option 2. An abstract has also been submitted to COSPAR on the work of this contract for presentation at that meeting. However, Dr. Maynard will not be able to attend without the augmentation.

Submitted to JGR 2/27/98

Electrodynamics of the inner magnetosphere observed in the dusk sector by CRRES and DMSP during the magnetic storm of June 4 - 6, 1991

W. J. Burke,[1] N. C. Maynard,[1] M. P. Hagan,[3] R. A. Wolf,[4] G. R. Wilson,[2] L. C. Gentile,[3] M. S. Gussenhoven,[1] C. Y. Huang,[3] T. W. Garner,[4] and F. J. Rich[1]

Short title: ELECTRIC FIELDS IN INNER MAGNETOSPHERE

Abstract. We compare equatorward/earthward boundaries of convection electric fields and auroral/plasma sheet electrons detected by the DMSP F8 and CRRES satellites during the June 1991 magnetic storm. Measurements come from the dusk magnetic local time sector where the ring current penetrates closest to the Earth. The storm was triggered by a rapid increase in the solar wind dynamic pressure accompanied by a southward turning of the interplanetary magnetic field (IMF). Satellite data show that: (1) All particle and field boundaries moved equatorward/earthward during the initial phase, probably in response to the strong southward IMF turning. (2) Electric field boundaries were either at lower magnetic L shells or close to the inner edge of ring current ions throughout the main and early recovery phases. Penetration earthward of the ring current occurred twice as the polar cap potential increased rapidly. (3) Electric potentials at subauroral latitudes were large fractions of the total potentials in the afternoon cell, twice exceeding 60 kV. (4) The boundaries of auroral electron precipitation were more variable than those of electric fields and mapped to lower L shells than where CRRES encountered plasma sheet electrons. Observations qualitatvely agree with predictions of empirical models for auroral electron and electric field boundaries.

Introduction

Empirical knowledge about the distribution of electric fields in the ionosphere and magnetosphere is critical for modelling global plasma transport during periods of high geomagnetic activity. The purpose of this paper is to describe the evolution of convective electric fields observed at high and low altitudes during the magnetic storm of June 4 - 6, 1991. Primary data come from the ion drift meter (IDM) on the Defense Meteorological Satellite Program Flight 8 (DMSP F8) satellite in the topside ionosphere and the electric field instrument (EFI) on the Combined Release and Radiation Effects Satellite (CRRES) near the equatorial plane of the magnetosphere. Supporting information is provided by particle spectrometers on both spacecraft and a magnetometer on CRRES. At various times during the storm the orbits of both satellites traversed the dusk magnetic local time (MLT) sector. The emphasis of this paper is on electric field penetration to low magnetic invariant latitudes, Λ in the ionosphere, and L shells in the magnetosphere. Comparisons between the two data sets are justified by the proximity of the two spacecraft in MLT and implemented through the simple mapping relationship between Λ and L in regions where the Earth's magnetic field usually is nearly dipolar.

It has long been known that storm-time electric fields couple the ionosphere at high and low latitudes. *Nopper and Carovillano* [1978] showed that the enhanced region 1 field-aligned currents of high magnetic activity periods cause the equipotentials of high latitude convection patterns to expand equatorward. For the purpose of this study it is useful to distinguish between two equipotential shapes that appear in Figure 1 of *Nopper and Carovillano* [1978]. The first looks similar to those found at auroral latitudes during moderate activity [*Heppner and Maynard*, 1987]. In the dusk sector the associated electric fields are mostly meridional, pointing poleward, and driving westward plasma convection. The second equipotential shape extends to much lower latitudes and is associated with zonal electric fields at equatorial latitudes [*Nopper and Carovillano*,

1978].

The distribution of electric fields in the magnetosphere affects the drifts of plasma constituents. The general features of electric field and particle boundaries can be understood in terms of convection theory. *Schield et al.* [1969] and *Vasyliunas* [1970; 1972] showed that the inner edge of the plasma sheet/ring current population tends to shield the inner magnetosphere from the convection electric field. Region 2 Birkeland currents flow along field lines threading the inner plasma sheet to support the shielding. In the plasma sheet and ring current, ions are more energetic than electrons and contribute more to the gradient-curvature drift component of the current [*Harel et al.*, 1981a, b]. Thus, ions play the dominant role in generating region 2 currents. When shielding is good the most earthward penetration of strong electric fields should roughly coincide with the inner edge of ring current ions.

Kavanagh et al. [1968] first showed that plasma sheet electrons drift closer to the Earth on the dawn than on the dusk side. Combined electric field and gradient-curvature drifts allow energetic ions to reach closer to the Earth in the dusk sector than electrons [*Chen*, 1970]. However, in the absence of sunlight, electron precipitation controls ionospheric conductance. This vanishes equatorward of the auroral electron boundary. Part of the post-dusk region 2 current flows along the ion inner edge into the low conductance part of the nightside ionosphere. *Southwood and Wolf* [1978] suggested that strong electric fields would be needed to drive ionospheric currents poleward from the ion inner edge to the high conductance auroral oval. These strong electric fields are among the most dramatic manifestations of shielding that appear at subauroral latitudes [*Smiddy et al.*, 1977; *Maynard et al.*, 1980] and rapid plasma drifts [*Galperin et al.*, 1973; *Anderson et al.*, 1993]. These phemomena are now commonly referred to as subauroral ion drift (SAID) events. They are characterized by intense electric fields ($\sim$100 mV/m) that are confined to narrow latitudinal ranges ($\sim$1°) in the post-dusk sector of the ionosphere. We show that in the large magnetic storm of June 4 - 6, 1991

the electron and ion boundaries become separated by more than 1°, In this case the elelectric field become spread out. DMSP F8 crossed only SAID structures and these were embedded in much broader regions of subauroral electric fields.

Shielding reflects adjustments in the positions and strengths of the storm-time ring current. The force balance equation near the equatorial plane of the inner magnetosphere $\nabla p = \mathbf{j} \times \mathbf{B}$, is well approximated by $\partial_{Rp} \approx \partial_R B^2/2\mu_0$. Here p and $\mathbf{j}$ represent the pressure and current density of the ring current; $\mathbf{B}$ is the Earth's magnetic field. The eastward and westward portions of the ring current are driven by oppositely directed pressure gradients in the radial profile of the ring current ions [*McEntire et al.*, 1985]. The location of the westward ring current's inner edge appears as a minimum in the profile of the difference between the magnitudes of the measured and the model magnetic field values [*Cahill*, 1973]. This corresponds to the maximum energy density or pressure of ring current ions [*Berko et al.*, 1975]. The weaker eastward ring current flows earthward of this location [see *Lui et al.*, 1987; *DeMichelis et al.*, 1997]. The principal energy density of the storm-time ring current is in the 24 - 300 keV range [*Smith and Hoffman*, 1973]. In the dusk-sector region of deepest ring current penetration, ion energy-versus-time spectrograms are characterized by "nose" shaped structures. On the spectrograms the "nose" energy is generally between 30 and 40 keV and is determined by the convection, corotation and gradient drifts [*Smith and Hoffman*, 1975]. The medium energy of quiet-time ring current ions is >300 keV [*Smith and Hoffman*, 1973].

Recent studies have focused on the effects of storm-time electric fields on plasma drifts in the equatorial ionosphere [*Spiro et al.*, 1988; *Fejer at al.*, 1990; *Scherliess and Fejer*, 1997; *Fejer and Scherliess*, 1997]. Techniques were developed to distinguish effects of penetrating zonal electric fields [*Nopper and Carovillano*, 1978] and of the storm-time dynamo [*Blanc and Richmond*, 1980]. In the strict sense used by Fejer and coworkers, "penetration" refers to not fully shielded electric fields whose ionospheric effects reach all the way to the magnetic equator. Unfortunately, neither DMSP nor CRRES can reliably

measure these relatively weak zonal electric fields. Given the measuring capabilities of the two spacecraft, in this paper we use the term "penetration" to describe electric fields (plasma drifts) that are detected equatorward of the boundary of low-energy auroral electron precipitation or earthward of the inner boundary of plasma sheet electrons regardless of the level of shielding by ring current ions.

Gussenhoven et al. [1981] reported that the equatorward boundary of auroral electron precipitation in the ionosphere is MLT dependent and strongly correlates with the level of geomagnetic activity. They interpreted this auroral boundary as the earthward boundary of the plasma sheet and showed that its variations are empirically well described by the Volland–Stern electric field model [*Volland*, 1975; *Stern*, 1975]. Best fits were obtained with the Volland-Stern parameter $\gamma \approx 2$. In this interpretation the equatorward auroral electron boundary maps the position of the zero-energy Alfvén boundary in the magnetosphere, the instantaneous separatrix between open and closed equipotentials in the magnetospheric equatorial plane. This boundary separates equipotentials that contact the magnetopause from those that circulate within the plasmasphere. The empirical fitting index γ describes the degree of penetration to the inner magnetosphere, $\gamma = 1$ corresponds to full penetration and $\gamma = \infty$ to full shielding [*Southwood and Kaye*, 1979].

The next section describes the DMSP F8 and CRRES orbits and the particle and field sensors on these spacecraft. The observations section first gives an overview of the June 4 - 6, 1991 magnetic storm. We then present and compare the DMSP and CRRES electric field and electron measurements. Electric field penetrations of the inner magneotsphere are also compared with locations of the ring current determined using CRRES magnetic field measurements. We show that during the main and early recovery phases of the storm, dipole mappings of auroral electron boundaries measured by DMSP in the ionosphere were consistently earthward of plasma sheet electron boundaries crossed by CRRES near the magnetic equator. The discussion section compares satellite

observations with the predictions of empirical models of auroral electron boundaries [*Gussenhoven et al.*, 1981] and magnetospheric electric fields [*Volland*, 1973; *Stern*, 1975]. Elements of the Volland–Stern model relevant to this study are described in an appendix.

Instrumentation

DMSP F8 is in a circular polar orbit at ~840 km that is sun-synchronous and lies close to the geographic dawn–dusk meridian. Because of the offset between the geographic and geomagnetic poles, the highest magnetic latitude (Λ_{max}) reached by the satellite differs in diurnally repeated patterns. Trajectories with $\Lambda_{max} \geq 80°$ occur between 2300 and 1200 UT. In the southern (northern) hemisphere the F8 trajectory generally crosses the magnetic noon–midnight meridian on the night (day) side of the dawn–dusk meridian. Data come from an ion drift meter (IDM), [*Rich and Hairston*, 1994] and an ion/electron spectrometer [*Hardy et al.*, 1984] that are identical to sensors previously flown on DMSP.

The IDM measures the horizontal and vertical components of plasma flow across the trajectory. The horizontal drift is driven by the meridional component of the electric field. The electric field parallel to the spacecraft's track can be calculated from the "frozen in flux" equation

$$\mathbf{E} = -\mathbf{v} \times \mathbf{B}$$

where E is the convection electric field, B is the geomagnetic field and v is the ion drift velocity. The electric field component along the spacecraft velocity vector is

$$E_{\text{parallel}} = (-v_{horiz} \cdot B_{vert}) + (-v_{vert} \cdot B_{horiz})$$

Integration of this electric field component gives the potential distribution along the trajectory.

$$\phi(L) = \int E_{\text{parallel}} \cdot dl$$

The limits of the integration are nominally set at 50° magnetic latitude on either side of the polar region. This assumes that $\phi = 0$ and $E = 0$ at mid-latitudes. This is not aways true. During significant geomagnetic activity, the limits are stepped equatorward in increments of 5° until $v \approx 0$. Also, if H^+ ions are present at 50°, a false $v \neq 0$ signal is received. If this condition is detected, a search is made to find a location where $v \approx 0$ poleward of 50° and equatorward of auroral activity. If such a location cannot be found, the pass is not processed. After a pass is initially processed the computed ϕ may not be zero. When this happens the ϕ distribution is adjusted with a linear trend that forces ϕ to zero at the end of the integration path. If the correction is large, then the results of the integration are usually ignored. At mid to high latitudes the vertical drift is mostly field aligned. At equatorial latitudes the zonal electric field component drives upward drifts that are usually too small to be measured reliably by the IDM.

Particle spectrometers on DMSP satellites measure fluxes of downcoming electrons and ions in the energy range from 30 eV to 30 keV, in 20 logarithmically-spaced steps. In this paper we are interested in electron measurements primarily to identify the low latitude boundary of auroral electron precipitation.

The CRRES satellite flew the most complete array of particle and field instrumentation ever assembled for investigations of the inner magnetosphere. It was launched in late July 1990 into an 18.2° inclination orbit with apogee at a geocentric distance of 6.3 R_E and perigee at an altitude of 350 km. The orbital period was about 10 hours. The satellite was spin stabilized at a rate of 2 rpm, with its spin axis pointing within 15° of the Sun. The local time of apogee during June 1991 was in the early evening sector. Of the scientific data compiled by CRRES, we are here concerned with measurements taken during outbound passes by the electric field instrument (EFI) [*Wygant et al.*, 1992], the low-energy plasma analyzer (LEPA) [*Hardy et al.*, 1993], and the magnetic field instrument (MFI) [*Singer et al.*, 1992]. During inbound passes inside the $L \approx 4$ magnetic shell, CRRES was in eclipse and these sensors were turned off to

conserve battery power.

The EFI on CRRES utilized a biased, double floating probe technique with both cylindrical and spherical sensors located on 100-m tip-to-tip wire antennas. Both types of sensors could be biased to optimize the impedance between the probes and the plasma and thus minimize errors. The bias currents effectively null photoemission currents to the sensors and minimize changes in floating potentials for small variations in collection current. Pointing the spin axis of CRRES toward the sun minimized photocurrent asymmetries. The two electric field measurement axes were in the spin plane approximately aligned with the solar-ecliptic Y and Z directions. The third component can be derived using the $\mathbf{E} \cdot \mathbf{B} = 0$ condition whenever the magnetic field vector lies more than 20° from the satellite's spin plane. Although the normal sampling rate is 32 s^{-1}, here we present spin-averaged measurements from the cylindrical probes using a least-squares fit to a sine wave over each satellite rotation.

The MFI on CRRES monitored variations in the Earth's magnetic field using a triaxial fluxgate magnetometer mounted at the end of a 6.1 m mast. The normal sampling rate was 16 s^{-1}. Two different gain ranges of $\pm 45,000$ nT and ± 900 nT allowed least significant bit resolution of 22 and 0.4 nT, respectively. The instrument is typically in high-sensitivity mode on all three axes over 75% of each CRRES orbit.

LEPA consisted of two triquadraspherical electrostatic analyzers with microchannel plate detectors to measure fluxes of electrons and ions with energies between 10 eV and 30 keV. During the CRRES mission the ion detector covered the full range of energies. Measurements from electron energy channels below 100 eV are not available. The analyzers had fields of view of 128° by 5.5°, and were mounted on the spacecraft to cover the range 30° to 150° with respect to the satellite's spin axis. The 128° field of view was divided into 16 zones of 8° width. Usually the detectors sampled fluxes both parallel and antiparallel to the Earth's magnetic field once per spin. The full energy range was swept 64 times per satellite spin. The detector thus sampled the complete

range of pitch angles for 0° to 180° every 15 s with a resolution of 5.5° by 8°.

Far more information was collected by LEPA than could be transmitted to ground with available telemetry. Thus, different two-dimensional cuts through the measurements giving energy/pitch-angle distributions were specified prior to launch. This paper utilizes data acquired in its most commonly used operating mode. The MFI readings were used to identify the LEPA zone whose plane of rotation contained the loss cone. For all cases studied LEPA telemetered 64 energy spectra per spin acquired in that zone. Data discussed here represent snapshots taken when that zone was looking perpendicular or parallel to the magnetic field.

Observations

This section has three parts. The first gives an overview of solar wind/IMF inputs and global magnetospheric responses during the magnetic storm of June 4 - 6, 1991. The second and third subsections give DMSP F8 and CRRES observations in the ionosphere and magnetosphere, respectively. To facilitate comparisons between the two spacecraft we reference measurements to invariant latitude Λ and magnetic L shell. We then illustrate our methods for identifying the inner boundaries of auroral/plasma sheet electron fluxes and electric fields. Examples given in Plates 1 and 2B were chosen for presentation because the satellites encountered the boundaries at nearly the same times. Consecutive high-latitude passes of DMSP indicate that the electric field and auroral electron boundaries were nearly stationary at the time of the example. Finally, we compare observed variations of the boundaries at the locations of the two spacecraft.

Environmental Overview

From top to bottom, Figure 1 plots as functions of UT on June 4 - 6, 1991, hourly averages of the the solar wind density n, and speed V, and five minute averages of the three components of the IMF, presented in standard geocentric solar magnetospheric

(GSM) coordinates. The data were taken by the IMP 8 satellite in the postnoon sector, prior to its entering the magnetosheath. For simplicity we adopt the notation 4/1200 UT in referring to 1200 UT on June 4, 1991. There are significant data gaps near 4/0954 – 1255, 5/0556 – 1010, and 5/1736 – 2057 UT. Solar wind data are not available for most of June 6. High resolution solar wind measurements show that at ~4/1530 UT V rapidly increased from ~460 km/s to 600 km/s. The variations in n and V indicate that the largest dynamic pressure of the solar wind occurred early on June 5. Simultaneous with the jump in V, IMF B_Z turned southward, and maintianed that polarity until ~4/2100 UT. Significant southward IMF turnings occurred near 5/0300, 5/1400, 5/23, 6/0100 and 6/0700 UT.

Information about global magnetospheric responses to the solar wind/IMF variations are presented in Figure 2. The top plot contains polar cap potentials, Φ_{pc}, estimated with the W–96 model (dashed line) from interplanetary parameters [*Weimer et al.*, 1996] and measured by DMSP F8 (triangles). Hash marked segments above these plots indicate times when $\Lambda_{max} \geq 80°$ and DMSP trajectories were favorably positioned to cross large fractions of Φ_{pc}. The second and third plots show values of the magnetic Kp and Dst indices. For later reference, the bottom plot gives the magnetic L shell location of CRRES during orbits 764 through 770. The letters E and e represent locations on outbound CRRES passes when EFI first encountered dawn-to-dusk electric fields and LEPA detected plasma sheet electron fluxes, respectively. During the prestorm orbit 764 the inner boundary of the plasma sheet was beyond CRRES apogee.

Storm initiation was detected as a 34 nT sudden storm commencement (SSC) at 4/1535 UT at the Ettayapuram station on the magnetic equator. Near this time the hourly averaged value of Dst increased from -1 to +11 nT. The initial phase ended after 4/1700 UT. The main phase is marked by three ring current injections with minimum magnetic deflections -50, -190 and -219 nT at 4/2200, 5/0800 and 5/2000 UT. Each of these ring current injections follows a southward excursion of IMF B_Z

(Figure 1). A maximum Kp of 9^- was reached between 5/1500 and 1800 UT. Attention is directed to the top plot which shows that polar cap potentials in excess of 100 kV were measured 15 times by DMSP F8 during the main and recovery phases of the storm. The largest potentials ~160 kV were detected at 5/0612 and 5/0936 UT. The W-96 model predicted values of $\Phi_{pc} > 200$ kV several times. The largest, ~250 kV, occurred when Kp = 9^-. However the DMSP F8 trajectory was not favorably located to cross most of the potential pattern. Surveys of ground and geostationary satellite data available on the World Wide Web from the National Geophysics Data Center (http://www.ngdc.noaa.gov/stp/stp.html) show that: (1) A substorm onset at 4/1545 UT was followed by nearly continuous geomagnetic activity at auroral latitudes, and (2) the magnetopause was at or inside goestationary altitude from about 4/2300 to 5/0700 UT and from 5/1500 to 5/1815 UT.

DMSP F8 Measurements

Plate 1 gives an example of DMSP F8 measurements taken at southern high latitudes in the early evening MLT sector between 5/0300 and 0310 UT. The presented data allow us to illustrate the methods by which electron precipitation and electric field penetration boundaries were determined. The top two plots contain directional differential fluxes of downcoming electrons and ions with energies between 30 eV and 30 keV in an energy versus time, color spectrogram format. The middle trace gives the horizontal component of plasma measured by the IDM, with effects due to corotation removed. Negative values correspond to sunward (westward) drifts.

The bottom plot gives the electrostatic potential distribution along the trajectory. The minimum potential of -51 kV at 0307:51 UT corresponds to the reversal in the plasma drift as the satellite crossed the ionospheric projection of the plasma sheet boundary layer (PSBL) [*Zeleyni et al.*, 1990; *Burke et al.*, 1994] into the polar cap.

The flux of electrons increased sharply at ~5/0306:11 UT from dayside photoelectron

to plasma sheet levels. We assign the auroral electron precipitation boundary to this time corresponding to an invariant magnetic latitude $\Lambda_e \approx 62°$. The magnetic L shell is determined by $L_e = 1/cos^2\Lambda_e$. We note that the ion precipitation boundary extends equatorward of Λ_e. The fact that average energies were decreasing at the time of first ion detection suggests that the boundary was one of DMSP energy sensitivity rather than a true precipitation boundary. We return to this point in discussing CRRES measurements near the magnetic equator. In some cases the low-latitude boundaries of electric fields are not as obvious as those for electrons. Boundaries are assigned to times when ion drifts deviate from steady baseline values measured at low magnetic latitudes. In this case the boundary is crossed between 5/0302:34 UT ($\Lambda_E = 50°$) and 5/0303:11 UT ($\Lambda_E = 52.6°$). Note that the bottom plot shows a potential maximum of ~2.2 kV at 5/0303:11 UT. This indicates the occurrence of a weak convection reversal not visible in the presented IDM data. However, the reversal is obvious when the IDM data are viewed at higher resolution. Whenever ambiguity exists about boundary locations we have assigned the higher magnetic latitudes. Thus, Λ_E and L_E values cited represent upper bounds. In each case we also used the assigned boundaries to estimate the fractions of the potential in the afternoon (negative potential) cell distributed in the auroral and sub-auroral latitudes. In the case shown in Plate 1 the potential crossed by DMSP F8 in the auroral oval was -28 kV, and at sub-auroral latitudes -23 kV.

The histories of Λ_E and Λ_e boundaries observed by DMSP F8 during the storm are given in Figure 3. The Dst trace is repeated for reference. The bottom plot shows that beginning at the time of the SSC Λ_E and Λ_e moved equatorward almost 15°. Most of this movement occurred during the initial phase (positive Dst) of the storm. However lowest values in the Λ_E trace at approximately 50°, 47° and 43°, occurred as Dst approached episodic minima during the storm's main phase. The Λ_e trace is similar to that of Λ_E, but appears to be more variable. The average separation between the two boundaries $\Delta\Lambda = |\Lambda_e - \Lambda_E|$ was $6.2° \pm 3.1°$, wuth values ranging from ranging

from ~1° at 4/0141 UT before the storm to 14° at 5/2150 UT during the last ring current injection when Dst was -213 nT. Some of the apparent rapid variations in Λ_e near 5/1200 UT reflect the fact that F8 often crossed auroral boundaries at significantly different magnetic local times in the northern and southern hemispheres [*Gussenhoven et al.*, 1981].

We note in passing that we were only able to identify in the DMSP F8 data set two rapid subauroral ion drift events, characterized by sunward plasma flows >2.5 km/s confined to latitudinal widths of ~1° [*Anderson et al.*, 1993]. Both events were detected in the southern (winter) ionosphere at 4/2022 and 5/0445 UT during portions of the main phase of the storm when Dst had negative slopes, suggesting new injections. Both structures were embedded within broader regions of subauroral electric fields. In neither case was CRRES at a location favorable for observing their magnetospheric signatures.

Figure 4 plots the distributions of potentials measured along the DMSP trajectories in crossing the afternoon convection cell. Each of these potentials is divided into two segments. The top (black) portions of the lines represent the potentials (Φ_a) in kilovolts measured in regions of auroral electron precipitation. The bottom (grey) portions give the penetration potentials (Φ_{pen}) measured between Λ_e and Λ_E. These data show that before the SSC the potentials were modest and mostly confined to the auroral oval. After onset the total potential increased as did the fraction at sub-auroral latitudes. As the main phase of the storm developed, Φ_{pen} consistently exceeded 30 kV. Twice Φ_{pen} reached 60 kV, at 5/1458 and 6/0935 UT during the second ring current injection of the main phase and a small recovery phase injection, respectively. The late recovery phase was characterized by a return to small potentials and relatively little subauroral penetration.

CRRES Measurements

Plate 2A shows CRRES measurements from the outbound part of orbit 765. The data are the Y_{GSE} component of the electric field (top) and directional differential fluxes of trapped electrons and ions measured by LEPA. E_Y is positive in the dawn-to-dusk direction. Not displayed are field-aligned fluxes for the two plasma species. Whenever plasma sheet electrons were detected, their fluxes were nearly isotropic. This is consistent with our assumption that the equatorward boundary of auroral electron precipitation maps to the earthward boundary of plasma sheet electrons. While significant ion fluxes were detected moving both ways along the magnetic field, the distributions were anisotropic, peaking at pitch angle near 90°.

This pass began shortly after the solar wind's dynamic pressure increased and the IMF turned southward (4/1430 UT) IMF (Figure 1). This was followed by a large increase in the predicted Φ_{pc} (Figure 2). E_Y was in the dawn-dusk direction throughout the pass which places the electric field penetration boundary at $L_E \leq 2.0$. Attitude errors did not allow accurate electric field measurements earthward of this point. The electric field was variable around the background magnitude of 1 - 2 mV/m. After 4/1700 UT the variations increased and the background reduced to $\leq$1 mV/m. Electron and ion boundaries detected by LEPA at 4/1735 ($L_e = 5.1$) and 4/1724 UT ($L = 4.85$) were relatively close together at the beginning of the main phase. There are two features to note. First, the electric field boundary was well earthward of both the electron and ion boundaries. This same characteristic was also seen later in the storm in orbit 769 when Φ_{pc} also increased rapidly. Second, the electron boundary was dispersionless in energy, characteristic of a very recent injection.

Plate 2B shows similar CRRES measurements during the outbound part of orbit 766 which encompasses the interval of the southern high latitude pass shown in Plate 1 (5/0300 - 0310 UT). Note that CRRES data were acquired near 1700 MLT; the DMSP orbit was close to the 1900 MLT meridian (Plate 1). The top plot shows that prior

to 5/0227 UT the electric field oscillated at low amplitudes about zero. Between then and 0244 UT the amplitude of E_Y grew in magnitude and its orientation was mostly dusk-to-dawn. From 0244 to 0400 UT E_Y was predominantly positive. We place the electric field boundary at $L_E \approx 3.75$ (0244 UT). The flux of low energy electrons rose above background at 0342 UT when CRRES was near $L_e = 5.4$. Not suprisingly for the dusk sector, the flux of low-energy ions reached significantly closer to the Earth than the plasma sheet electrons. We note that the inner edge of ion detection roughly corresponded to the reversal in E_Y. The energy-versus-time structure of ions shown in the lower spectrogram of Plate 2B suggests that these are the so called "nose" component of the ring current [*Smith and Hoffman*, 1974]. If so, ring current ions with energies >30 keV extended earthward of the first ion detection by LEPA. Three items should be noted. First, within the plasma sheet the amplitudes of electric field variations were very large, but are of no concern for the present study. Second, the electric field reversal at 0244 UT corresponds to what should be encountered while crossing a sheet of positive space charge. Third, the potential difference between the locations of the electric field and plasma sheet electron boundaries, obtained by integrating the electric field along the CRRES trajectory is -15.4 kV. Comparing these with data shown in Plate 1, we tentatively identify the small positive potential region in the ionosphere with the dusk-to-dawn E_Y region. The penetration electric field measured by DMSP between Λ_E and Λ_e should correspond to the dawn-to-dusk E_Y detected by EFI between L_E and L_e. The ion data presented in Plate 2B are representative of several of the orbits in this storm. Their earthward boundaries were inside L_e, and they were close to the locations of L_E and reversals in the polarity of E_Y. During the late recovery phase (orbit 770) they were clearly inside of L_E.

Figure 5 presents the difference between the magnetic field magnitude measured by CRRES and that predicted by the International Geomagnetic Reference Field (IGRF) model (solid lines) and the integrated potential along CRRES trajectories (dashed

lines) for the seven orbits. The electric field, plasma sheet electron and westward ring current (L_R) particle boundaries are marked on the figure. Since CRRES orbits take several hours to cover the plotted spatial intervals, we caution that temporal and spatial variations may be mixed. However, the ring current is of such large dimensions that we may safely assume that its variations are primarily spatial. The minima in ΔB marked by L_R indicate the inner edges of the westward ring current and the negative slopes in ΔB earthward of the minima denote the eastward ring currents [*Cahill*, 1973]. If overshielding by the ring current occurred, the potential reached a maximum at L_E then turned negative, as in orbit 766 (Plate 2B). The positive potential excursions (most obvious in orbit 768) were always small and are not always apparent on scales chosen to emphasize the negative potentials inside of L_e. In each case Φ_{pen} values measured by CRRES were comparable in magnitude to those measured by DMSP (Figure 4).

The following characteristics should be noted in Figure 5. (1) No plasma sheet ion or electron boundaries were crossed during orbit 764. The quiet-time ring current is associated with $>$ 300 keV ions [*Smith and Hoffman*, 1973]. (2) The storm-time ring current was first encountered during orbit 765. It pushed earthward through the time of orbit 768 when Dst reached its minimum value (Figure 2). During the recovery phase the ring current's inner edge retreated slowly. (3) The ion boundary measured by LEPA and the inner edge of the ring current followed each other closely [*Berko et al.*, 1975]. (4) The electron boundary moved in the opposite direction to the ring current boundary. Its apparent outward motion is due in part to the inflation of magnetic flux tubes caused by the ring current. (5) L_E penetrated earthward of all particle boundaries during rapid increases in Φ_{pc} (orbits 765 and 769). At other times it retreated to (orbits 766 and 770) and even beyond (orbit 768) the ion boundary when shielding was established. Overshielding, in the form of dusk-to-dawm electric field (positive potential) excursions occurred near the inner ion boundary. The electric field structure is consistent with the presence of very small quantities of positive space charge. (6) Oscillatory structures in

the ΔB and E_Y measurements of orbit 767 occurred during a lull in geomagnetic activity after a long period of large Φ_{pc}. L_E is placed at 2.0, although a period of dawn-to-dusk electric field was encountered just earthward of $L = 2.85$. Radially oscillating structures are commonly detected in the ring current [*De Michelis et al.*, 1997].

Data presented in Figure 6 show how magnetospheric locations of the electric field (open diamonds) and plasma sheet electron (open triangles) boundaries detected by CRRES changed over the course of the storm. The plot shows that CRRES L_E decreased from 4.5 before the storm to 2.0 during the initial phase, then oscillated between this value and 3.7 before retreating to 4.3 at the time of orbit 770. Detection of relatively low and high L_E values by CRRES during the storm occurred near the middle and ends of UT days, respectively. As mentioned previously CRRES did not enter the plasma sheet in the orbit prior to the storm onset. During the initial phase orbit 765, the boundary appeared at $L_e = 5.1$, then migrated to larger values during the main and early recovery phases. The plasma sheet electron fluxes detected near $L_e = 4$ late in the recovery phase (orbit 770) are weak and anisotropic, peaking at pitch angles near 90°. They appear to be remnants of an earlier injection [*Burke et al.*, 1995].

To facilitate comparison between CRRES and DMSP F8 measurements, we have also plotted in Figure 6 dipole mappings of Λ_E (closed diamonds) and Λ_e (closed triangles) taken at comparable universal times. Looking first at the mapping of the electric field, we see that DMSP L_E also decreased rapidly during the initial phase of the storm onset then remained earthward of $L = 3$ with relatively small UT diurnal fluctuations during the main and early recovery phases. At the time of the CRRES orbit 770 both satellites measured similar values of L_E. The mapping of L_e shows some of the variability noted in Figure 3. However, until late in the storm recovery the mapped values of L_e were consistently earthward of detections by CRRES in the magnetosphere.

It appears possible that the empirical discrepancy between detections of L_e in the magnetosphere and ionosphere reflects magnetic local time variations of electron

guiding center drift paths. For example, *Gussenhoven et al.* [1981] showed that during high geomagnetic activity the equatorial boundary of auroral electron precipitation is at highest magnetic latitudes in the late afternoon MLT sector. This explanation requires that CRRES measurements were systematically made at earlier MLTs than DMSP, in the late afternoon sector. To test this hypothesis Figure 7 gives the distributions of L_E and L_e measurements by both satellites in an MLT/L polar plot format. The same symbols are used as in Figure 6. These data show that while L_E detections by CRRES were systematically at earlier MLTs than DMSP, this is not true for L_e encounters. In a few cases the L_e boundaries were crossed by the two satellites at approximately the same universal and magnetic local times. Even in these instances, their dipole mappings to the equatorial plane were significantly separated (Figure 6). We conclude that while a UT/MLT beating between the CRRES and DMSP F8 orbits may explain some of the small differences between measured L_E boundaries, another explanation must be sought to resolve the much larger L_e discrepancies. The most likely explanation involves the inflationary effects of the storm-time ring current (Figure 5) on magnetic field mapping between the ionosphere and the magnetic equator. We have calculated the equatorial mappings of Λ_e data points shown in Figure 6 using the *Tsyganenko* [1989] (T-89) magnetic field model with appropriately high Kp inputs. During the main and early recovery phases the T-89 mappings of Λ_e are in essential agreement with CRRES detections of L_e in the magnetosphere. Late in the recovery phase when the ring current had diminished, the equatorial mappings of CRRES (orbit 770) and DMSP encounters with the plasma sheet and auroral electron boundaries were very close to one another.

Discussion

The magnetic storm of June 4 - 6, 1991 had characteristics that were both ordinary and ideosynchratic. Signatures of standard initial, main, and recovery phases of the storm are evident in the Dst trace. The strong southward turning of the IMF at the

time of the increase in the dynamic pressure of the solar wind near 4/1530 UT probably hastened the transition from the initial to the main phase [*Craven et al.*, 1986]. However, the Dst trace also indicates that the development of the main phase ring current was interrupted several times by partial recoveries. A comparison with data in Figure 1 shows that these occurred during northward excursions of IMF B_Z.

The evolution of L_E relative to the ion and electron boundaries and the ring current distribution helps clarify the controlling electrodynamics. Explaining this complex geomagnetic storm and the electrodynamic responses of the inner magnetosphere requires the full power of computer simulations and is beyond the scope of this observational report. Indeed, simulations of the storm are underway using the Rice Convection Model and preliminary results have been reported by *Garner et al.* [1997]. Here we seek to provide simple physical explanations of the behaviors of the boundaries as observed in DMSP and CRRES data.

Electric field and electron boundary relationships

The electric field and the auroral electron boundaries showed distinctive responses to changing interplanetary conditions. Data in Figure 3 show that at ionospheric altitudes these boundaries reached their lowest invariant latitude near 5/0600 and 5/1800 UT, times when Dst had relatively large negative slopes, ~2 hours before reaching minimal values. Caution must be exercised in the apparently simple task of comparing low-energy electron with electric field boundaries. Magnetospheric electrons drift along trajectories that conserve total energy E, as well as the first ($\mu = mv_\perp^2/2B$) and second ($J = \int p_{||}, ds$) adiabatic invariants. Allowed drift paths are affected by the magnetic field geometry and the combined convective and corotational electric fields. Recall that the corotation electric field was removed from measurements presented above for ease in comparing the measurements from the two data sets and relating them to high-latitude, ionospheric electric-field models.

This subsection develops a semi-quantitative framework for understanding relationships between the two sets of measurements in terms of an empirical model for auroral electron boundaries [*Gussenhoven et al.*, 1981] and the Volland-Stern electric field model. To do this, it is useful to review two background concepts about superposed electric fields and electron drift paths in the magnetosphere.

Figure 8 schematically represents the distribution of electric equipotentials in the magnetosphere with and without the contribution of corotating magnetic field lines. Figure 8A shows a uniform dawn-to dusk electric field $\mathbf{E_0}$ yielding equipotentials whose equatorial projections are uniformly distributed along the Sun-Earth line. In this representation all equipotentials begin on the reconnection line in the magnetotail and end on the dayside magnetopause. We refer to these as open equipotentials. The equatorial projections of equipotential lines produced by a rotating magnetic dipole are closed circles. Figure 8B schematically represents superposed equipotentials due to $\mathbf{E_0}$ and a rotating magnetic dipole. Equipotentials have two topologies, open and closed.

Consider the equatorial projection of the drift path of an electron specified by (E, μ, J). In the distant magnetotail it primarily moves earthward under the influence of $\mathbf{E_0}$. As it convects into the inner magnetosphere the azimuthal component of drift increases due to the growing strengths of the magnetic gradient-curvature forces and the corotation electric field. For electrons with any (E, μ, J) the equatorial plane is divided into regions of allowed and forbidden drift paths, which may either close on themselves or reach the magnetopause. The separatrix between open and closed trajectories for electrons with a given (E, μ, J) is commonly referred to as their Alfvén boundary. The Alfvén boundaries for low energy electrons lie closer to the Earth than for electrons with higher energies. Of particular interest are the drift paths of electrons with very low kinetic energy which essentially follow equipotential lines. The zero-energy Alfvén boundary lies just outside of the last closed equipotential line in Figure 8B.

In the following paragraphs we compare CRRES and DMSP observations with

the predictions of a very simple representation of the Volland–Stern electric field. *Gussenhoven et al.* [1981] showed that the low-latitude boundary of auroral electron precipitation in a given MLT sector correlates with the Kp index and that its dipole mapping to the magnetospheric equatorial plane is well approximated as the zero-energy Alfvén boundary predicted by the Volland–Stern model. Thus, an immediate comparison of one major aspect of the present CRRES and DMSP measurements is appropriate. In the appendix we develop equations for the Volland–Stern model with a uniform dawn-to-dusk electric field that fully penetrates the inner magnetosphere. Equations (4A) and (5A) show that the shape of the zero-energy Alfvén boundary and the electric potential distribution within it are specified by the ratio of the polar cap potential (Φ_{pc}) to the stand off distance of the subsolar magnetopause L_{ss}.

Before comparing our results with model predictions it is useful to recognize that (1) *Gussenhoven et al.* [1981] correlated Λ_e with the Kp index, (2) Volland–Stern is a vacuum electric field model which does not explicitly include plasma effects, and (3) equipotentials in the magnetotail are relatively uniformly distributed as sketched in Figure 8 [*Maynard et al.*, 1995]. Nevertheless these empirical models provide useful guidance for estimating boundary locations and potential distributions in the inner magnetosphere. Even their failures help understand the dynamic effects of the ring current on the evolution of these quantities.

Figure 9 plots Λ_e (bottom) and its dipole mapping L_e (top) as observed by DMSP F8 with the predictions of the *Gussenhoven et al.* [1981] model. The calculations used the Kp regression relations appropriate to the MLT sectors in which DMSP crossings of the auroral boundaries occurred (Table 2 of *Gussenhoven et al.* [1981]). A comparison of data points contained in the figure supports the following conclusions: (1) The Kp-driven, calculated values of Λ_e and L_e moved equatorward/earthward faster in the storm's initial phase than is indicated in DMSP F8 auroral boundary measurements. (2) During the storm's main phase the calculated values of L_e hovered between 3

and 3.5. Occasionally the measured boundaries penetrated to these values. Observed electron boundaries were much more variable than predicted by *Gussenhoven et al.* [1981]. The differences partly reflect rapid boundary responses to changes in the driving electrodynamics due to IMF variations. The three hour index Kp was insensitive to such rapid variations during the storm. (3) As the ring current decayed during the recovery phase, predicted and calculated boundary locations were in substantial agreement. Interplanetary measurements are not available for this period to help clarify the few obvious discrepancies late on June 6.

In the appendix on the Volland–Stern electric field model we show that the zero-energy Alfvén boundary and the penetration potential within it are specified by the ratio Φ_{pc}/L_{ss}. The empirical electric field model of *Weimer* [1996] was used to estimate Φ_{pc} (Figure 2). The standoff distance was estimated using the dynamic pressure of the solar wind (Figure 1). Values of L_{ss}, computed for times when interplanetry measurements are available, are presented in the top plot of Figure 10. The calculations indicate that several times during the storm's main phase L_{ss} was at or near geostationary altitude. The hash-marked boxes in the top plot of Figure 10 indicate times when measurements from LANL or GOES satellites show that the magnetopause was inside geostationary orbit. The middle plot gives the magnetic L shell of the zero-energy Alfvén boundary using Φ_{pc} and L_{ss} and the the MLT at which DMSP F8 crossed Λ_e. During the storm's main phase the calculated value of L_e ranged between 2 and 3.5.

The bottom plot of Figure 10 contains predicted and measured values of the penetration potentials. The calculations were based on equation (5A) and used the MLTs at which DMSP F8 crossed Λ_E and Λ_e. Data selected for presentation were randomly chosen based on their proximity in time to calculations of Φ_{pc} and L_{ss}. The data show many of the qualitative features of the Volland–Stern model predictions. While four measured data points exceed 40 kV, the maximum potentials predicted by the model are closer to 30 kV.

Equation (5A) inticates that the largest penetration potentials should be detected close to the dusk meridian. Figure 11 shows scatter a plot of Φ_{pen} measured by DMSP F8 versus MLT. The largest values of Φ_{pen} were indeed detected just sunward of the dusk meridian. To check the validity of this observational result we have examined, but do not show, Λ_E and Λ_e measurements by sensors on the DMSP F9 satellite during the storm. This satellite is in sun-synchronous polar orbit near the 1030 - 2230 geographic local time meridian. Near the 2100 MLT meridian the electric field distribution was similar to that observed by DMSP F8 in this sector. However, on orbits near the midnight MLT meridian DMSP F9 detected no separations between the Λ_E and Λ_e boundaries.

To help quantify the degree of agreement between the observations and models, we have reproduced information contained in Figures 9 and 10 as scatter plots in Figure 12. Data in the top plot give invariant latitudes of auroral boundaries as observed and predicted by *Gussenhoven et al.* [1981]. The middle plot shows dipole mappings of these boundaries compared with the predictions of the Volland–Stern model. Although this shows that regression coefficients are similar, agreement is better for the *Gussenhoven et al* [1981] model. The bottom plot correlates observations with Volland–Stern predictions of Φ_{pen}. In this case the regression coefficient was 0.8, and as shown in Figure 10, the model tends to underpredict the penetration potential. Since magnetic inflation caused the measured L_e vaules to be outside of their predicted locations, this is not surprising.

Electric field relationships to ion boundaries and the ring current

The previous subsection considered relationships between the potential that penetrates inside the zero energy electric field boundary to the ratio of Φ_{pc}/L_{ss}. The relationship of L_E to the ion and ring current boundaries helps understand the physics controlling the potential distribution and shielding. Two very different penetration characteristics of the electric field relative to the ring current boundary L_R are found in

the passes displayed in Plate 2.

During orbit 765 (Plate 2A) dawn-dusk electric fields were observed to $L = 2$, the earthward limit for valid electric field measurements during this pass. These data were acquired just after the sudden commencement and during the time when the ring current was being established (see Figure 2 for DST and Figure 5 for the *in situ* magnetic field disturbance). The ion and electron boundaries are close together and relatively dispersionless. The inner edge of the ion detection is just earthward of the minimum ΔB, or the inner edge of the storm-time ring current. The magnetosphere was responding to a sudden large increase in Φ_{pc}, predicted by the *Weimer* [1996] model to be ~200 kV. Under these conditions the dawn-dusk electric field penetrated the plasmasphere similar to free space. The penetration potential determined by both CRRES (Figure 5, plot 2) and DMSP (Figure 4 at 4/1730 UT) is ~30 keV. No shielding is evident. Penetration to L shells earthward of EFI's ability to make measurements also occurred on orbit 769. This pass occurred at a time in the recovery phase of the storm when rapid increases in Φ_{pc} (Figure 2) and Φ_{pen} were observed by DMSP.

In our presentation of CRRES measurements in Plate 2b and Figure 5, we noted that during the main and early recovery phases of the storm, L_E was otherwise close to the boundary for detecting ring current ions. The 30 keV high-energy limit for detecting ions by LEPA does not allow us to quantify the exact inner boundary. However, ion spectrograms suggest that LEPA detected the low-energy branches of the "nose" structures reported by *Smith and Hoffman* [1974]. *Chen* [1970] and *Stern* [1975] calculated the drift paths of low-energy protons in the magnetospheric equatorial plane. With a dipole magnetic field and the Volland–Stern fitting parameter $\gamma = 1$, the guiding centers of particles with equatorial pitch angles of 90° move along trajectories of constant

$$\Psi(R,\phi) = -\frac{\Omega B_0 R_E^3}{R} + E_0 R sin\phi + \frac{\mu B_0 R_E^3}{qR^3}$$

where R is the radial distance from the center of the Earth and ϕ is the local

time measured from midnight. Other symbols represent: the Earth's spin velocity $\Omega = 7.3 \times 10^{-5}$ s^{-1}, the surface magnetic field at the equator $B_0 = 3.1 \times 10^4$ nT, the radius of the Earth $R_E \approx 6.4 \times 10^6$ m, and the elementary charge of a proton or electron $q = \pm 1.6 \times 10^{-19}$ C. For a given value of E_0 there is a critical value for the magnetic moments of protons μ_{crit}. If $\mu < \mu_{crit}$, protons drift along trajectories with forbidden regions similar in form to those of low-energy electrons. If $\mu > \mu_{crit}$, ions gain access to regions closer to the Earth than the zero-energy Alfvén boundary. *Berko et al.* [1975] showed that the maximum magnetic deflection coincides with the peak of the ring current ions. Since these two boundaries approximately track each other in Figure 5, our ion boundaries determined from the LEPA data are nearly at the nose. The inner edges of the ring current and the protons in the dusk sector should also be related to the effective penetration distance of the storm time electric field. The electric field reverses at the ion boundary in Plate 2B to dusk-dawn before settling to near zero at very low L shells. The negative electric field is in the region of the weaker, inner eastward ring current. The electric field configuration inside the zero-energy Alfvén boundary is consistent with a weak positive space charge located at the inner edge of the westward ring current. This slight overshielding was seen clearly in orbits 766 and 768, and weakly in orbits 764 and 770. In all cases, except the two orbits which experienced the rapid increase in Φ_{pc}, most of the penetration potential drop occurs between the ion and electron boundaries. The distribution of electric fields is related to the separation of the allowed regions for the ion and electron populations.

Particle boundary separation and the ring current

From Figure 5 it is easy to see that as L_R moved earthward the ring current strengthened and the electron boundary moved outward. The reverse relative motion occurred during the recovery phase. A significant part of this apparent separation, especially the outward movement of L_e, results from the inflation of the inner

magnetosphere by the ring current. Inflation of the dipole determined the locations in L at which CRRES encountered boundaries and distorted the mapping of boundaries sampled by DMSP and plotted in the bottom plot on Figure 3.

Summary and Conclusions

In this paper we have compared electric field and charged particle boundaries detected by the DMSP F8 and CRRES satellites in the dusk MLT sector during the magnetic storm of June 4 - 6, 1991, at ionospheric and magnetospheric altitudes. The storm was initiated by a sudden increase in the dynamic pressure of the solar wind and a southward turning of the IMF. Early reactions were to compress the magnetosphere and impose a large potential across the polar cap. This potential caused electric field and auroral/plasma sheet electron boundaries to move equatorward/earthward in the ionosphere/magnetosphere. Comparisons of electric field boundaries with ring current locations show that: (1) Electric fields penetrated inside the ring current when the polar cap potential underwent strong and rapid increases. (2) At other times the electric field boundaries were close to the earthward boundaries of the ring current, where signatures of weak overshielding were detected.

The equatorward boundary of auroral electron precipitation mirrored the behavior of the electric field boundary throughout the storm, but showed a higher degree of variability. After its initial inward motion the earthward boundary of plasma sheet electrons retreated during the main and early recovery phases of the storm. These apparently disparate motions of auroral and plasma sheet boundaries illustrate the inflationary effects of the storm-time ring current on magnetic mapping between the ionosphere and the equatorial plane of the magnetosphere.

Appendix: The Volland–Stern Model

The Volland–Stern model represents the potential distribution, Φ, in the magnetospheric equatorial plane as the superposition of contributions from the interplanetary medium and by an Earth-centered, rotating magnetic dipole

$$\Phi(R,\phi) = -\frac{\Omega B_0 R_E^3}{R} + CR^{\gamma} sin\phi \qquad (1A)$$

The fitting parameter γ reflects the degree of electric field shielding [*Southwood and Kaye*, 1979]. With $\gamma = 1$, there is no shielding and the constant C represents a uniform dawn to dusk electric field $\mathbf{E_0}$. Equipotentials associated with such an electric field, in the absence of the corotation field, are represented in Figure 8a as uniformly spaced straight lines.

The corotation electric field is radially toward the Earth. Associated equipotential lines are Earth-centered circles. Along the dusk meridian line ($\phi = 3\pi/2$) the two electric fields point in opposite directions. At some distance R_S along this line the superposed fields exactly cancel. Defined in units of Earth radii

$$L_S = \frac{R_S}{R_E} = \sqrt{\frac{\Omega B_0 R_E^2}{E_0 R_E}} \qquad (2A)$$

Southwood and Kaye [1979] showed that the shape of the last closed equipotential, regarded as the zero-energy Alfvén boundary, L_A, is given by the expression

$$L_A(\phi) = \frac{L_S}{\left[1 + \sqrt{2}\left|cos\left(\frac{\phi - \pi \ over 2}{2}\right)\right|\right]} \qquad (3A)$$

Any point on the last closed equipotential $(X_A, Y_A) = (L_A(\phi)cos\phi,\ L_A(\phi)sin\phi)$.

From Figure 8a we see that $E_0 \approx \Phi_{pc}/W$, where Φ_{pc} is the potential imposed by the solar wind across the polar cap and W is the width of the magnetosphere along the dawn-dusk line. It is interesting to note that equatorial projections of the magnetopause determined from empirical studies have been shown to be self similar on the dayside [*Elsen and Winglee*, 1997], and that the subsolar distance $W \approx 3L_{ss}$ [*Howe and Binsack*,

1972; *Roelof and Sibeck*, 1993]. The corotation potential $\Phi_c = \Omega B_0 R_E^2$ is approximately 90 kV. Combining terms in (2A) we find that

$$L_S \approx \sqrt{\frac{3\, L_{ss}\, \Phi_c}{\Phi_{pc}}} \tag{4A}$$

With a storm-time polar cap potential of 200 kV and the subsolar magnetopause compressed to geostationary altitude $L_S \approx 3$.

The electric potential Φ_{pen} distributed inside of the last closed equipotentials ($L_A(\phi)$) is simply $-E_0, Y_A$. Combining terms we find that for the Volland–Stern model

$$\Phi_{pen} = \sqrt{\frac{\Phi_{pc}\Phi_c}{3L_{ss}}} \left[\frac{sin\,\phi}{1 + \sqrt{2}\left|cos\left(\frac{\phi - \frac{\pi}{2}}{2}\right)\right|} \right] \tag{5A}$$

Equations (3A), (A), and (5A) show that the zero-energy Alfvén boundary and the penetration potential are completely specified by the polar cap potential and the standoff distance of the subsolar magnetopause in the $\gamma = 1$ Volland–Stern model.

Acknowledgments. This work was supported in part by the U.S. Air Force Office of Scientific Research task 2311PL013 and by Air Force contract F19628-96-K-0030 with Boston College. Research at Mission Research Corporation and Rice University was supported under NASA grant NAG5-3182. The authors thank H. J. Singer of the NOAA Space Environment Center for helpful comments on the manuscript.

References

Anderson, P. C., W. B. Hanson, R. A. Heelis, J. D. Craven, D. N. Baker, and L. A. Frank, A proposed production model of rapid subauroral ion drifts and their relationship to substorm evolution, *J. Geophys. Res., 98*, 6069, 1993.

Berko, F. W., L. J. Cahill, Jr., and T. A. Fritz, Protons as the prime contributors to storm time ring current, *J. Geophys. Res., 80*, 3549, 1975.

Blanc, M., and A. D. Richmond, The ionospheric disturbance dynamo, *J. Geophys. Res., 85*, 1669, 1980.

Burke, W. J., J. S. Machuzak, N. C. Maynard, E. M. Basinska, G. M. Erickson, R. A. Hoffman, J. A. Slavin, and W. B. Hanson, Auroral signatures of the plasma sheet boundary layer in the evening sector, *J. Geophys. Res., 99*, 2489, 1994.

Burke, W. J., A. G. Rubin, D. A. Hardy, and E. G. Holeman, Banded electron structures in the plasmasphere, *J. Geophys. Res., 100*, 7759, 1995.

Cahill, L. J., Jr., Magnetic storm inflation in the evening sector, *J. Geophys. Res., 78*, 4724, 1973.

Chen, A. J., Penetration of low energy protons deep into the magnetosphere, *J. Geophys. Res., 75*, 2458, 1970.

Craven, J. D., L. A. Frank, C. T. Russell, E. J. Smith, and R. P. Lepping, Global auroral responses to magnetospheric compressions by shocks in the solar wind: Two case studies, in *Solar Wind-Magnetospheric Coupling* ed. by Y. Kamide and J. A. Slavin, Terra Sci. Publ. Co., Tokyo, 367, 1986.

De Michelis, P., I. A. Daglis, and G. Consolini, Average terrestrial ring current derived from AMPTE/CCE-CHEM measurements, *J. Geophys. Res., 102*, 14,103, 1997.

Elsen, R. K., and R. M. Winglee, The average shape of the magnetopause: A comparison of three-dimensional global MHD and empirical models, *J. Geophys. Res., 102*, 4799, 1997.

Fejer, B. G., and L. Scherliess, Empirical models of storm time equatorial zonal electric fields, *J. Geophys. Res., 102*, 24,047, 1997.

Fejer, B. G., R. W. Spiro, R. A. Wolf, and J. C. Foster, Latitudinal variation of perturbation electric fields during magnetically disturbed periods: 1986 SUNDIAL observations and model results, *Ann. Geophys., 8*, 441, 1990.

Galperin, Yu. I., V. N. Ponamarev, and A. G. Zosimova, Direct measurements of drift rate of ions in the upper atmosphere during a magnetic storm II. Results of measurements during magnetic storm of November 3, 1967, *Kosmicheski Issled., 11*, 273, 1973.

Garner, T. W., R. A. Wolf, R. W. Spiro, W. J. Burke, and N. C. Maynard, Simulation of the June 4 - 6 magnetic storm with the Rice Convection Model, *EOS, Trans. Am. Geophys. U., 78*, SA41A-1, F519, 1997.

Gussenhoven, M. S., D. A. Hardy, and W. J. Burke, DMSP/F2 electron observations of equatorial auroral boundaries and their relationship to magnetospheric electric fields, *J. Geophys. Res., 86*, 768, 1981.

Hardy, D. A., D. W. Walton, A. D. Johnstone, M. P. Gough, A. Huber, J. Pantazis, and R. Burkhardt, The low energy plasma analyzer, *IEEE, Trans. Nuclear Sci., 40*, 246, 1993.

Hardy, D. A., L. K. Schmidt, M. S. Gussenhoven, F. J. Marshall, H. C. Yeh, T. L. Shumaker, A. Huber, and J. Pantazis, *Precipitating electron and ion detectors (SSJ/4) for the block 5D/Flights 4-10 DMSP satellites: Calibration and data presentation*, Rep. AFGL-TR-84-0317, Air Force Geophysics Laboratory, Hanscom Air Force Base, MA, 1984.

Harel, M., R. A. Wolf, P. H. Reiff, R. W. Spiro, W. J. Burke, F. J. Rich, and M. Smiddy, Quantitative simulation of a magnetospheric substorm, 1. Logic and overview, *J. Geophys. Res., 86*, 2217, 1981a.

Harel, M., R. A. Wolf, R. W. Spiro, P. H. Reiff, C.-K. Chen, W. J. Burke, F. J. Rich, and M. Smiddy, Quantitative simulation of a magnetospheric substorm, 2. Comparison with observations, *J. Geophys. Res., 86*, 2242, 1981b.

Heppner, J. P., and N. C. Maynard, Empirical high-latitude electric field models, *J. Geophys. Res., 92*, 4467, 1987.

Howe, H. C., Jr., and J. H. Binsack, Explorer 33 and 35 plasma observations of magnetosheath flow, *J. Geophys. Res., 77*, 3334, 1972.

Kavanagh, L. D., Jr., J. W. Freeman, Jr., and A. J. Chen, Plasma flow in the magnetosphere, *J. Geophys. Res., 73*, 5511, 1968.

Lui, A. T. Y., R. W. McEntire, and S. M. Krimigis, Evolution of the ring current during two geomagnetic storms, *J. Geophys. Res., 92*, 7459, 1987.

Maynard, N. C., T. L. Aggson, and J. P. Heppner, The plasmaspheric electric field as measured by ISEE 1, *J. Geophys. Res., 88*, 3981, 1983.

Maynard, N. C., T. L. Aggson, and J. P. Heppner, Magnetospheric observations of large sub-auroral electric fields, *Geophys. Res. Lett., 7*, 881, 1980.

Maynard, N. C., W. F. Denig, and W. J. Burke, Mapping ionospheric convection patterns to the magnetosphere, *J. Geophys. Res., 100*, 1713, 1995.

McEntire, R. W., A. T. Y. Lui, S. M. Krimigis, and E. P. Keath, AMPTE/CCE energetic particle composition measurements during the September 4, 1984 magnetic storm, *Geophys. Res. Lett., 12*, 317, 1985.

Nopper, R. W., and R. L. Carovillano, Polar-equatorial coupling during magnetically active periods, *Geophys. Res. Lett., 5*, 699, 1978.

Rich, F. J., and M. Hairston, Large-scale convection patterns observed by DMSP, *J. Geophys. Res., 99*, 3827, 1994.

Roelof, E. C., and D. G. Sibeck, Magnetopause shape as a bivariate function of interplanetary magnetic field B_Z and solar wind dynamic pressure, *J. Geophys. Res., 98*, 21,421, 1993.

Scherliess, L., and B. G. Fejer, Storm time dependence of equatorial disturbance dynamo zonal electric fields, *J. Geophys. Res., 102*, 24,037, 1997.

Schield, M. A., J. W. Freeman, and A. J. Dessler, A source for field-aligned currents at auroral latitudes, *J. Geophys. Res., 74*, 247, 1969.

Singer, H. J., W. P. Sullivan, P. Anderson, F. Mozer, P. Harvey, J. Wygant, and W. McNeil, Fluxgate magnetometer instrument on CRRES, *J. Spacecr. Rockets, 29*, 599, 1992.

Smiddy, M., M. C. Kelley, W. Burke, F. Rich, R. Sagalyn, B. Shuman, R. Hays, and S. Lai, Intense poleward directed electric fields near the ionospheric projection of the plasmapause, *Geophys. Res. Lett., 4*, 543, 1977.

Smith, P. H., and R. A. Hoffman, Ring current particle distributions during the magnetic storms of December 16-18, 1971, *J. Geophys. Res., 78*, 4731, 1973.

Smith, P. H., and R. A. Hoffman, Direct observations in the dusk hours of characteristics of the storm time ring current particles during the beginning of magnetic storms, *J. Geophys. Res., 79*, 966, 1974.

Southwood, D. J., and R. A. Wolf, An assessment of the role of precipitation in magnetospheric convection, *J. Geophys. Res., 83*, 5227, 1978.

Southwood, D. J., and S. M. Kaye, Drift boundary approximations in simple magnetospheric convection models, *J. Geophys. Res., 84*, 5773, 1979.

Spiro, R. W., R. A. Wolf, and B. G. Fejer, Penetration of high-latitude electric field effects to low latitudes during SUNDIAL 1984, *Ann. Geophys., 6*, 39, 1988.

Stern, D. P., The motion of a proton in the equatorial magnetosphere, *J. Geophys. Res., 80*, 595, 1975.

Tsyganenko, N. A., A magnetospheric magnetic field model with a warped tail current sheet, *Planet. Spac Sci., 35*, 5, 1989.

Vasyliunas, V. M., Mathematical models of magnetospheric convection and its coupling to the ionosphere, in *Particles and Fields in the Magnetosphere*, ed. by B. M. McCormac, Series D, Reidel, Hingham, MA, 60, 1970.

Vasyliunas, V. M., The interrelationship of magnetospheric processes, in *The Earth's Magnetospheric Processes*, ed. by B. M. McCormac, Series D, Reidel, Dordrecht, 29, 1972.

Volland, H., Semiempirical model of large scale magnetospheric electric fields, *J. Geophys. Res., 80*, 595, 1975.

Weimer, D. R., A flexible, IMF dependent model of high latitude electric potentials having "space weather" applications, *Geophys. Res. Lett., 23*, 2549-2552, 1996.

Wygant, J. R., P. R. Harvey, F. S. Mozer, N. C. Maynard, H. Singer, M. Smiddy, W. Sullivan, and P. Anderson, The CRRES electric field/Langmuir probe instrument, *J. Spacecr. Rockets, 29*, 601, 1992.

Zelenyi, L. M., R. A. Kovrazkhin, and J. M. Bosqued, Velocity-dispersed ion beams in the nightside auroral zone: AUREOL-3 observations, *J. Geophys. Res., 95*, 12,119, 1990.

W. J. Burke, M. S. Gussenhoven, and F. J. Rich, Air Force Research Laboratory, 29 Randolph Road, Hanscom AFB, MA 01731-3010. e-mail: burke@plh.af.mil; gussen@plh.af.mil; rich@plh.af.mil

L. C. Gentile, M. P. Hagan, and C. Y. Huang, Boston College Institute for Scientific Research, 402 St. Clement's Hall, 140 Commonwealth Avenue, Chestnut Hill, MA 02167-3862. e-mail: gentile@plh.af.mil; mphagan@bc.edu; huang@plh.af.mil

N. C. Maynard and G. R. Wilson, Mission Research Corporation, One Tara Blvd., Suite 302, Nashua, NH 03062. nmaynard@mrcnh.com; gwilson@mrcnh.com

R. A. Wolf, Department of Space Physics and Astronomy, Rice University, Houston, TX 77005.

Received Month xx, 1998; revised Month xx, 1998; accepted Month xx, 1998.

---

[1]Air Force Research Laboratory, Hanscom Air Force Base, Massachusetts.

[2]Mission Research Corporation, Nashua, New Hampshire.

[3]Boston College Institute for Scientific Research, Chestnut Hill, Massachusetts.

[4]Department of Space Physics and Astronomy, Rice University, Houston, Texas.

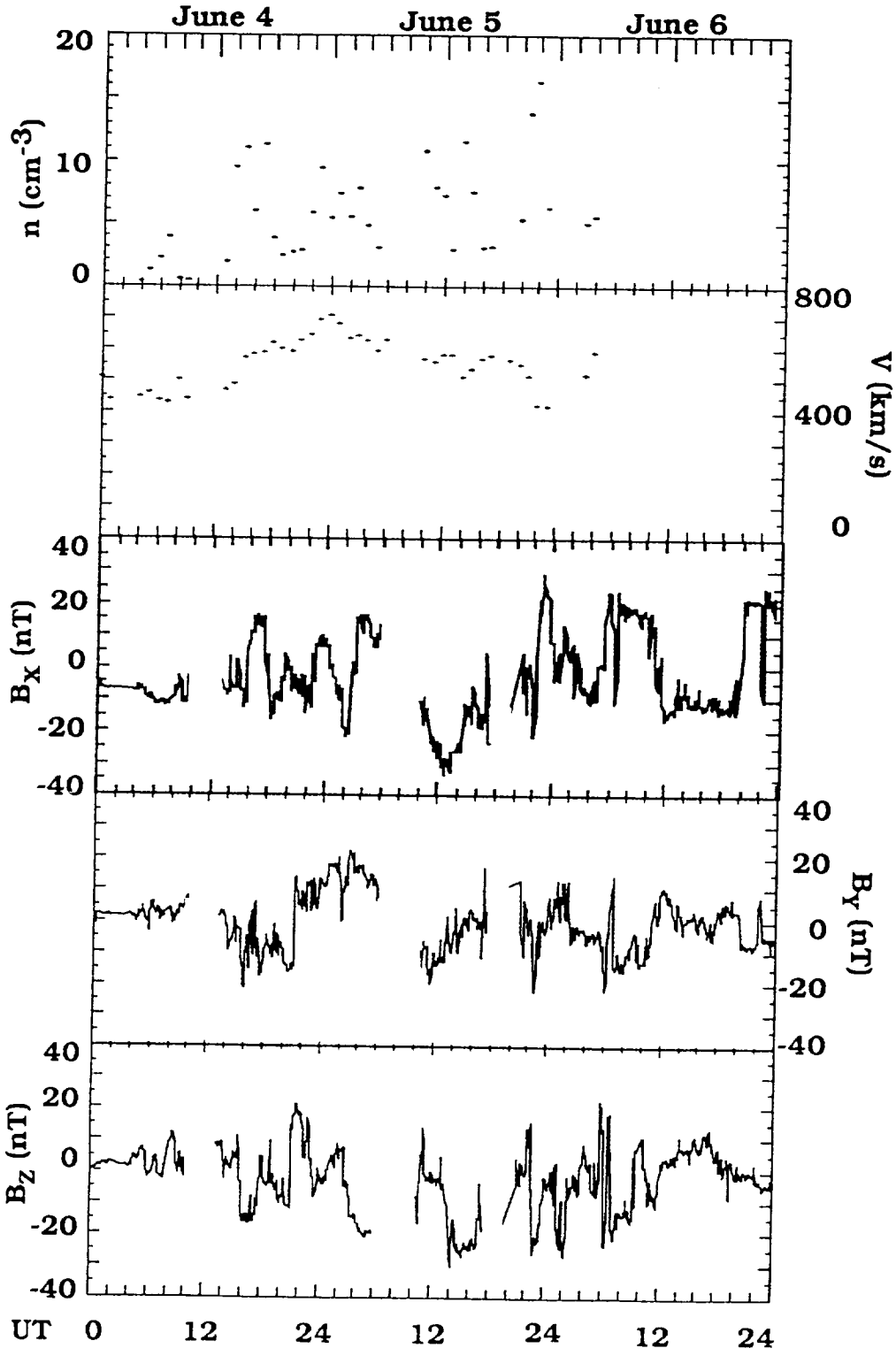

Figure 1. Solar wind density and speed and three components of the IMF measured by

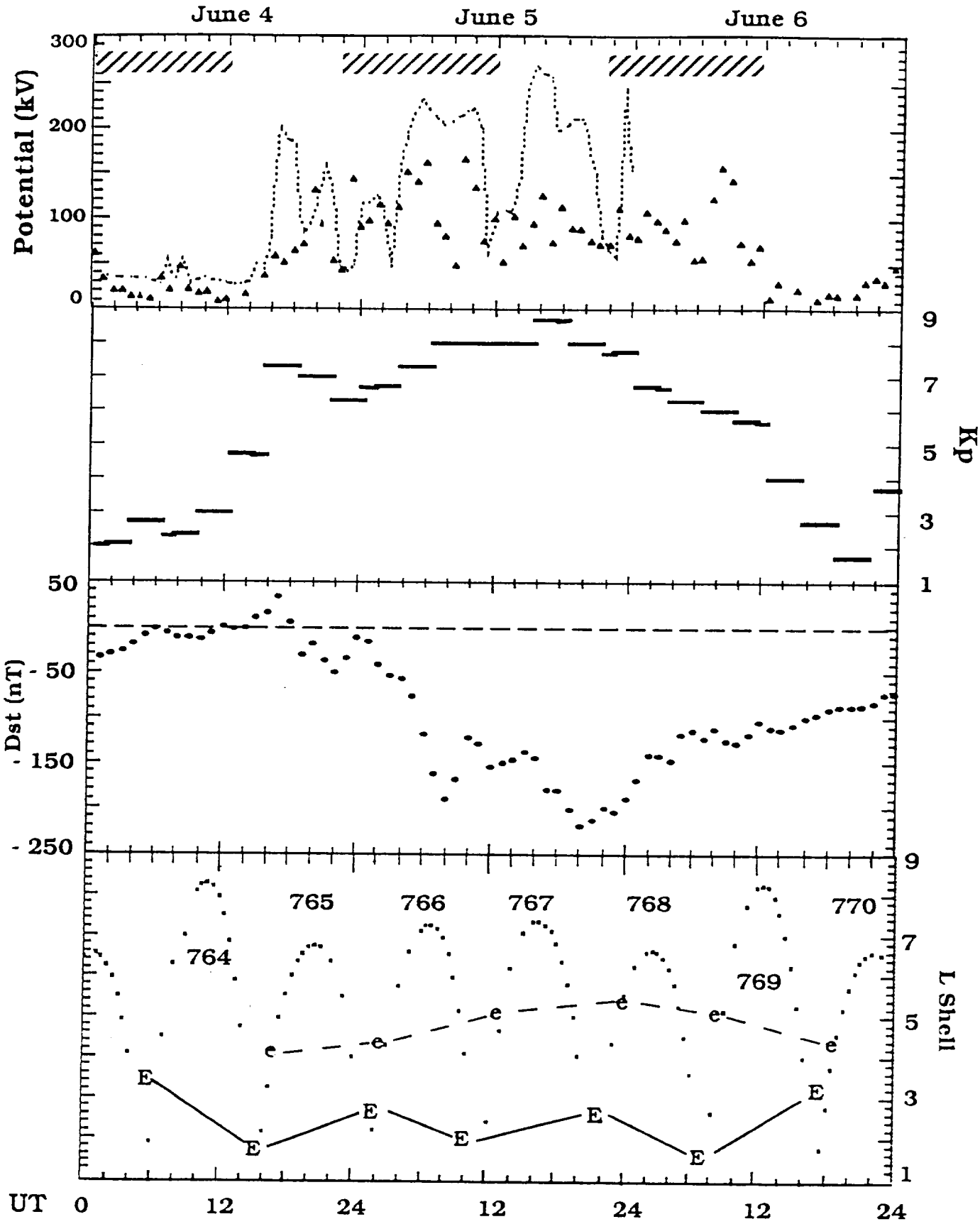

Figure 2. Magnetospheric response to interplanetary variations on June 4 - 6, 1991. The top plot contains DMSP measurements (triangles) and W-96 model predictions (dashed lines) of the polar cap potential. The second and third plots give Dst and Kp for the three days. The bottom plot indicates L shell locations of CRRES as well as the electric field (E) and plasma sheet electron (e) boundaries crossed during outbound orbital segments.

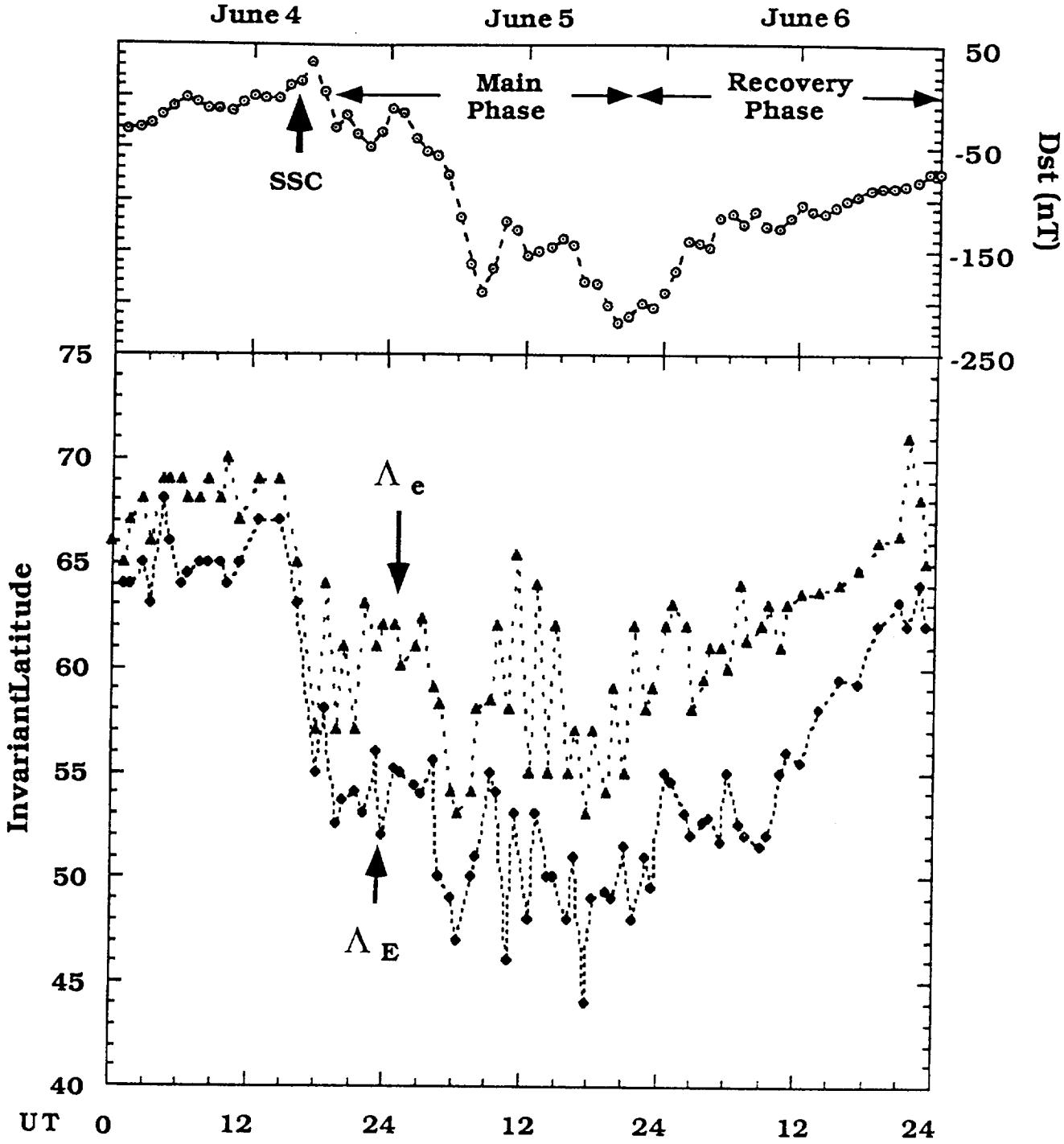

Figure 3. Plots of Λ_e and Λ_E observed by DMSP as a function of UT on June 4 - 6, 1991. The plot of Dst is repeated for comparison.

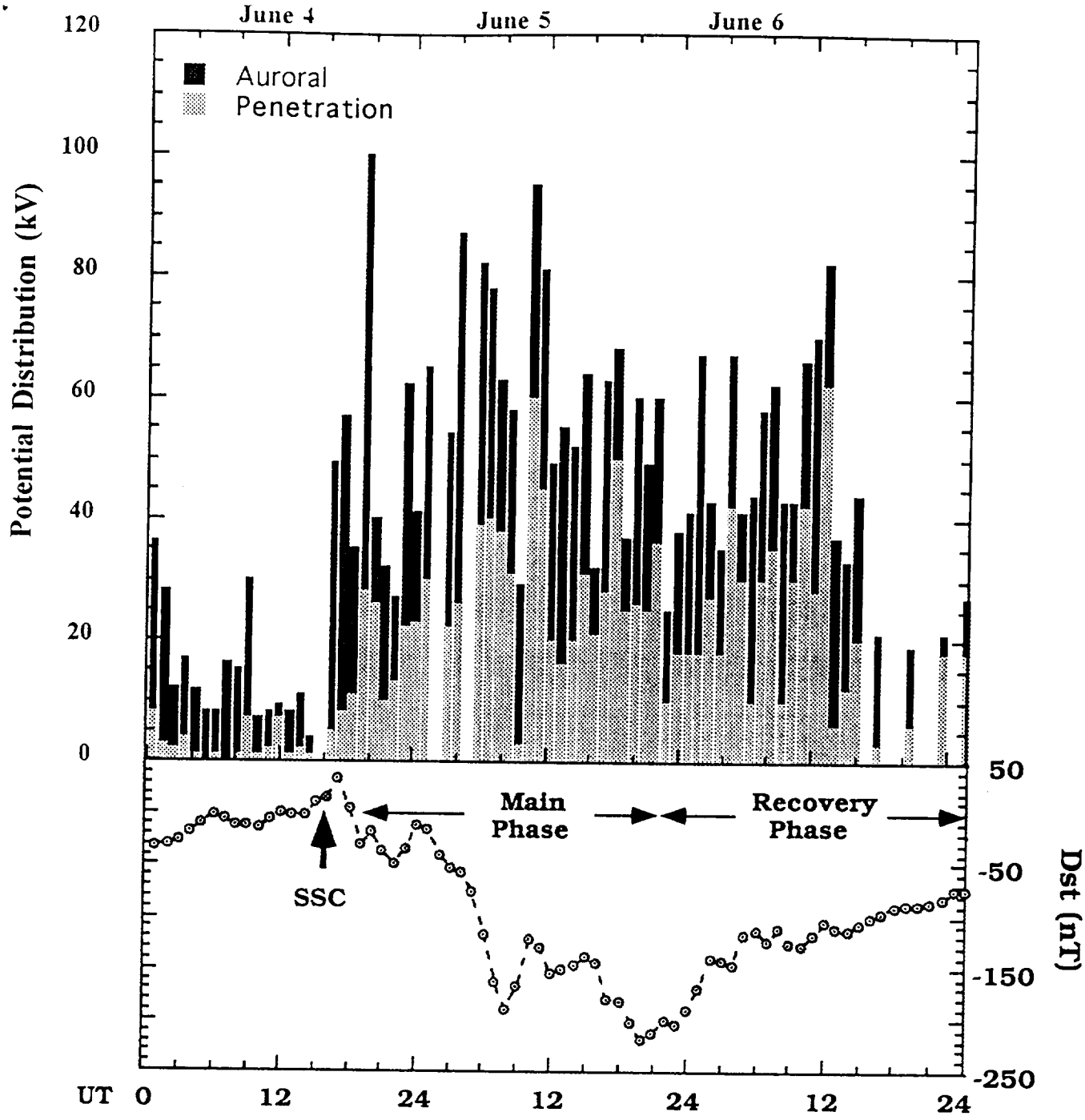

Figure 4. Distribution of potentials measured by DMSP F8 at auroral (black) and subauroral (grey) latitudes in the evening MLT sector during the June 4 - 6, 1991 storm.

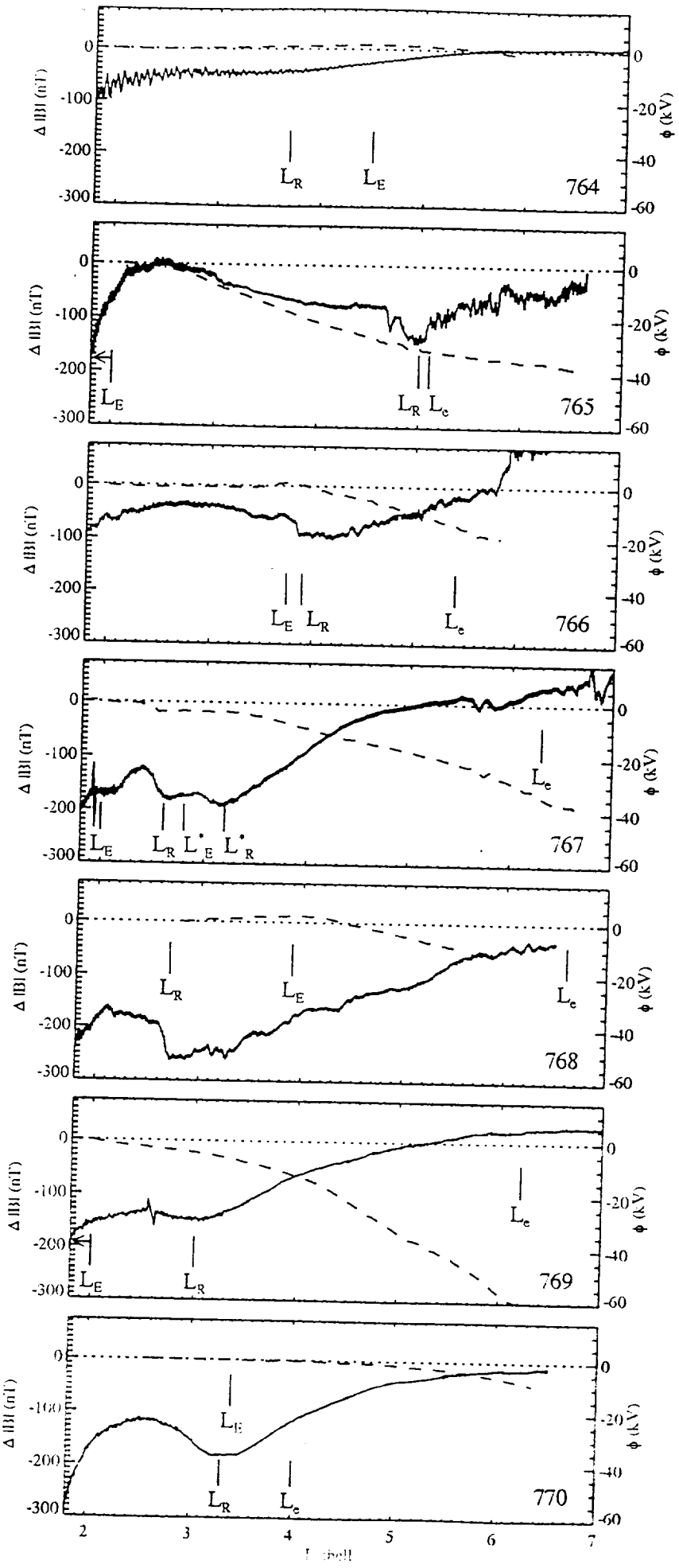

Figure 5. Profiles versus L of the difference between the measured magnitude of the magnetic field and the IGRF field model (solid lines), and of the integrated potential along the trajectory (dashed lines) for CRRES orbits covering from before the sudden commencement well into the recovery phase. The potential integration was truncated in several orbits when the angle between the satellite spin plane and the magnetic field became too small to calculate the electric field component along the spin axis. The L shell boundaries for electric fields (E), ions (p), electrons (e) and ring current (R) are marked for reference.

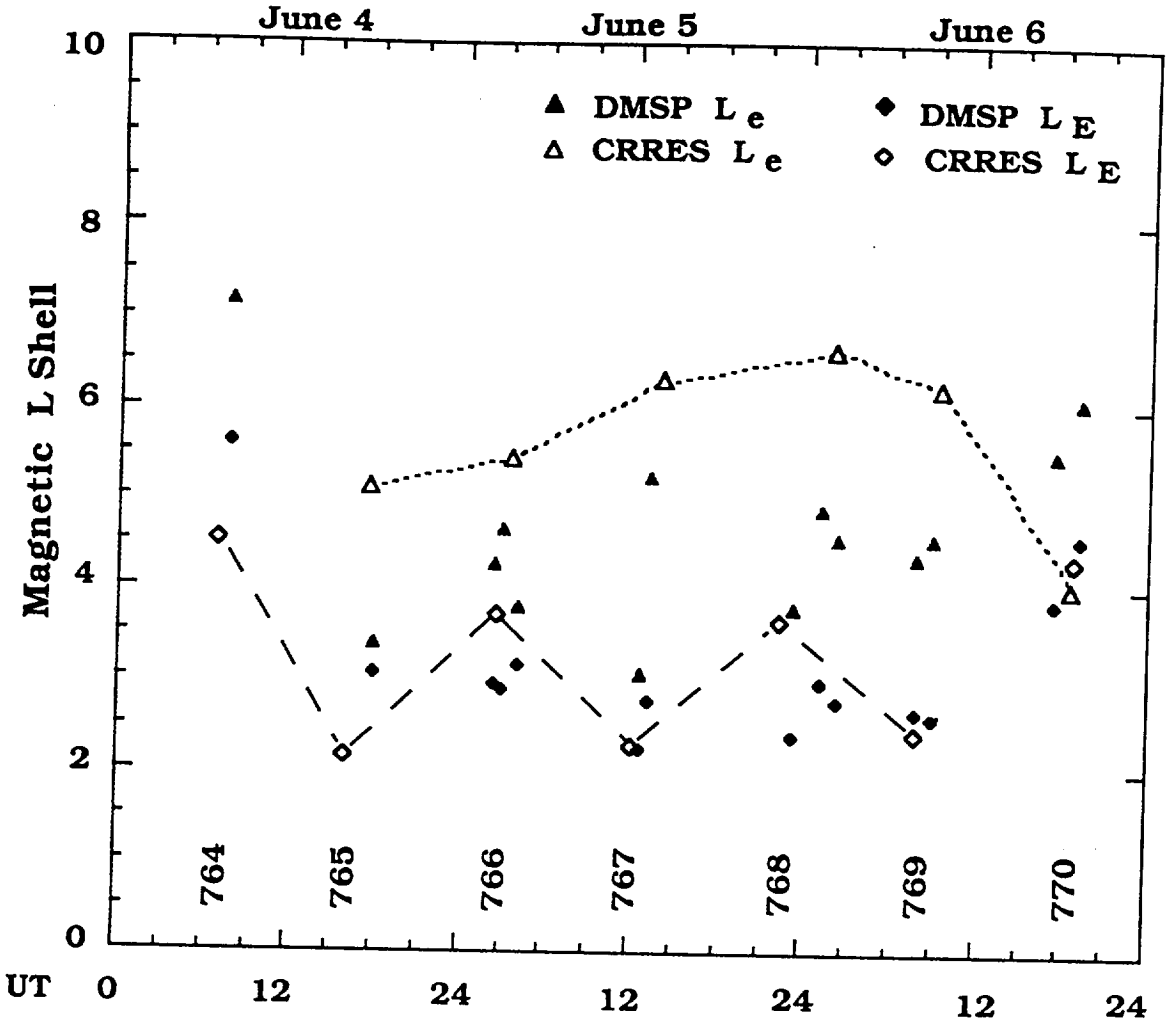

Figure 6. Magnetic L shells for detecting electric field (open diamonds) and plasma sheet electron (open triangles) boundaries detected by CRRES as functions of UT. Also plotted are the dipole mappings of these boundaries as measured by DMSP in the ionosphere at about the same time as the CRRES data.

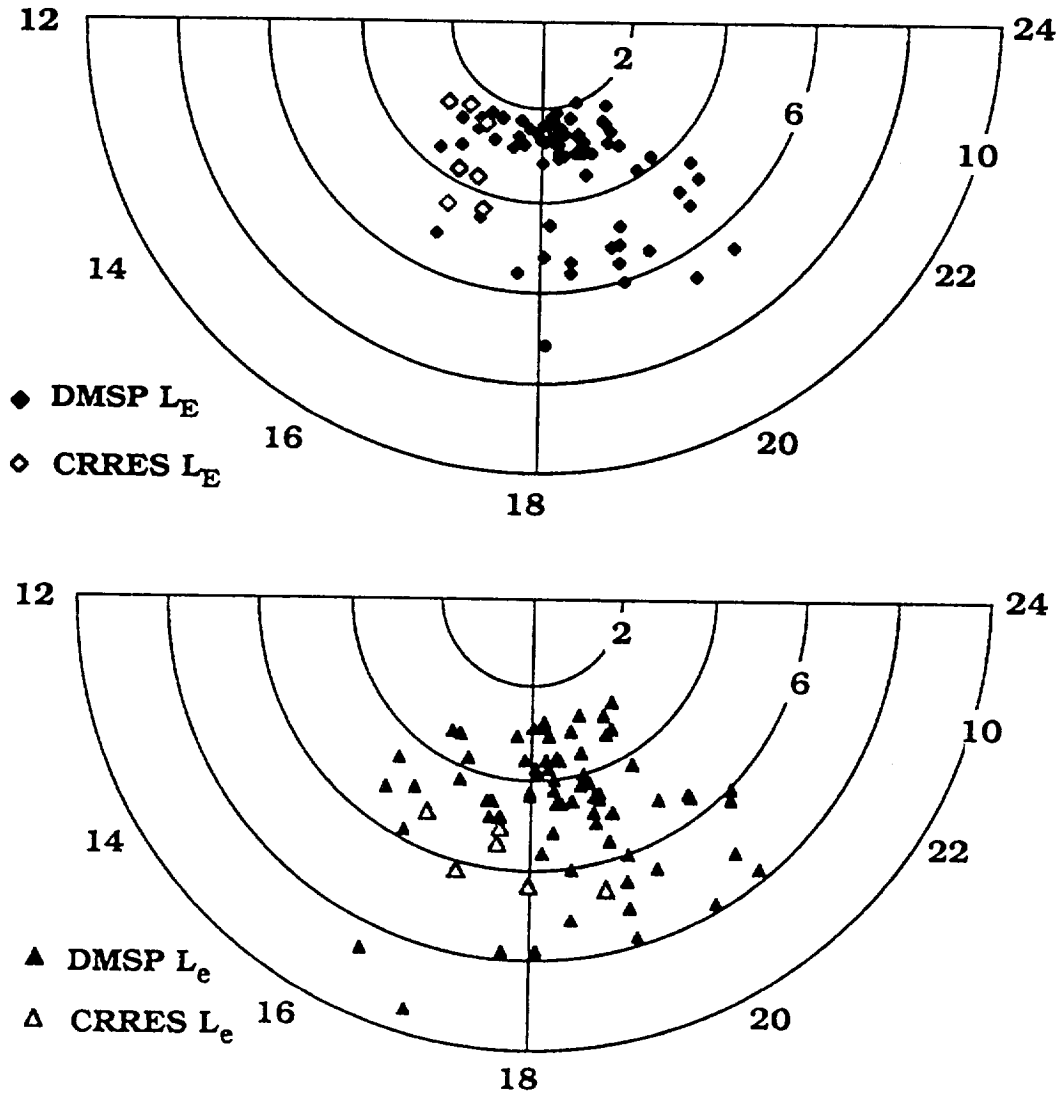

Figure 7. L versus MLT polar plots of locations for CRRES and DMSP F8 encounters with electric field (top) and electron (bottom) boundaries. Symbols have the same significance as in Figure 5.

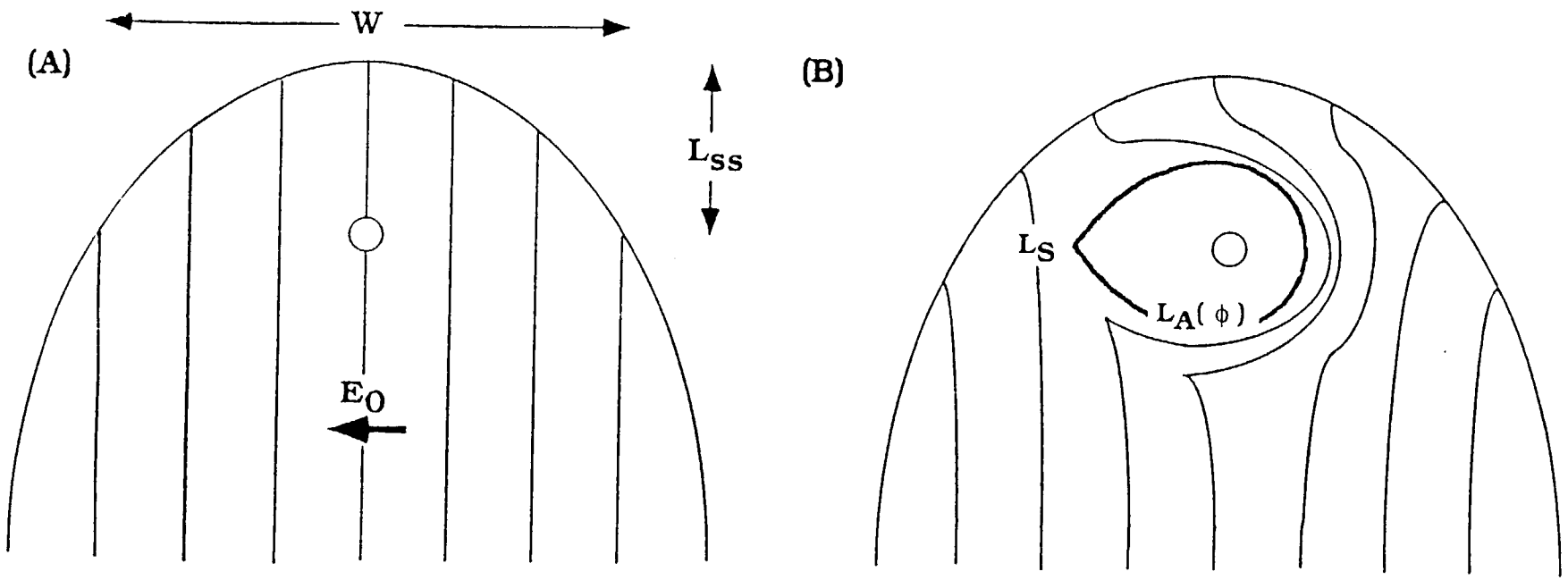

Figure 8. Schematic representation of the distribution of equipotentials in the magnetosphere. Plots (B) and (A) show the equipotentials with and without the corotation electric field. Symbols W, L_{ss}, L_S and $L_A(\phi)$ represent the width of the magnetosphere along the dawn–dusk line, the standoff distance to the subsolar magnetopause, the stagnation point, and the last closed equipotential, respectively.

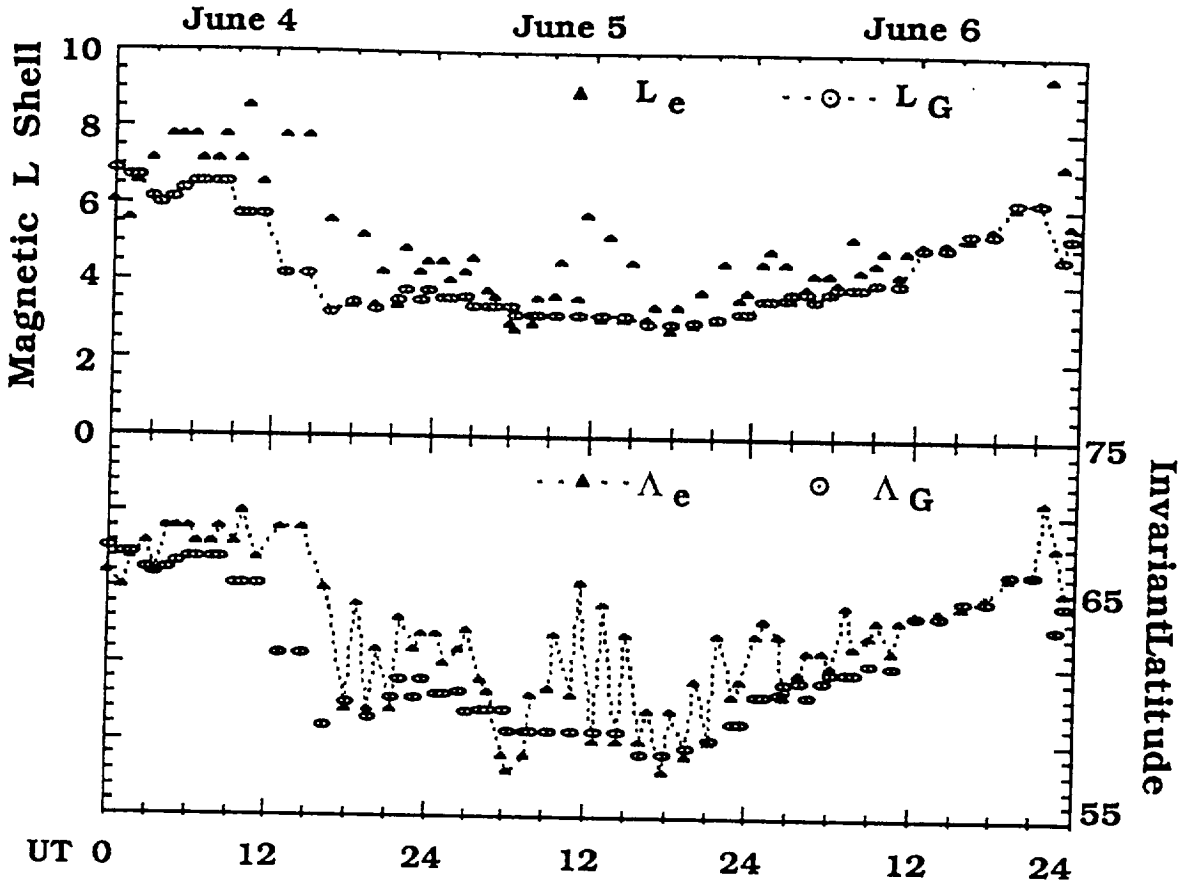

Figure 9. Comparisons of L_e (top) and Λ_e (bottom) measured by DMSP F8 with values predicted by *Gussenhoven et al.* [1981] for the June 4 - 6, 1991 magnetic storm.

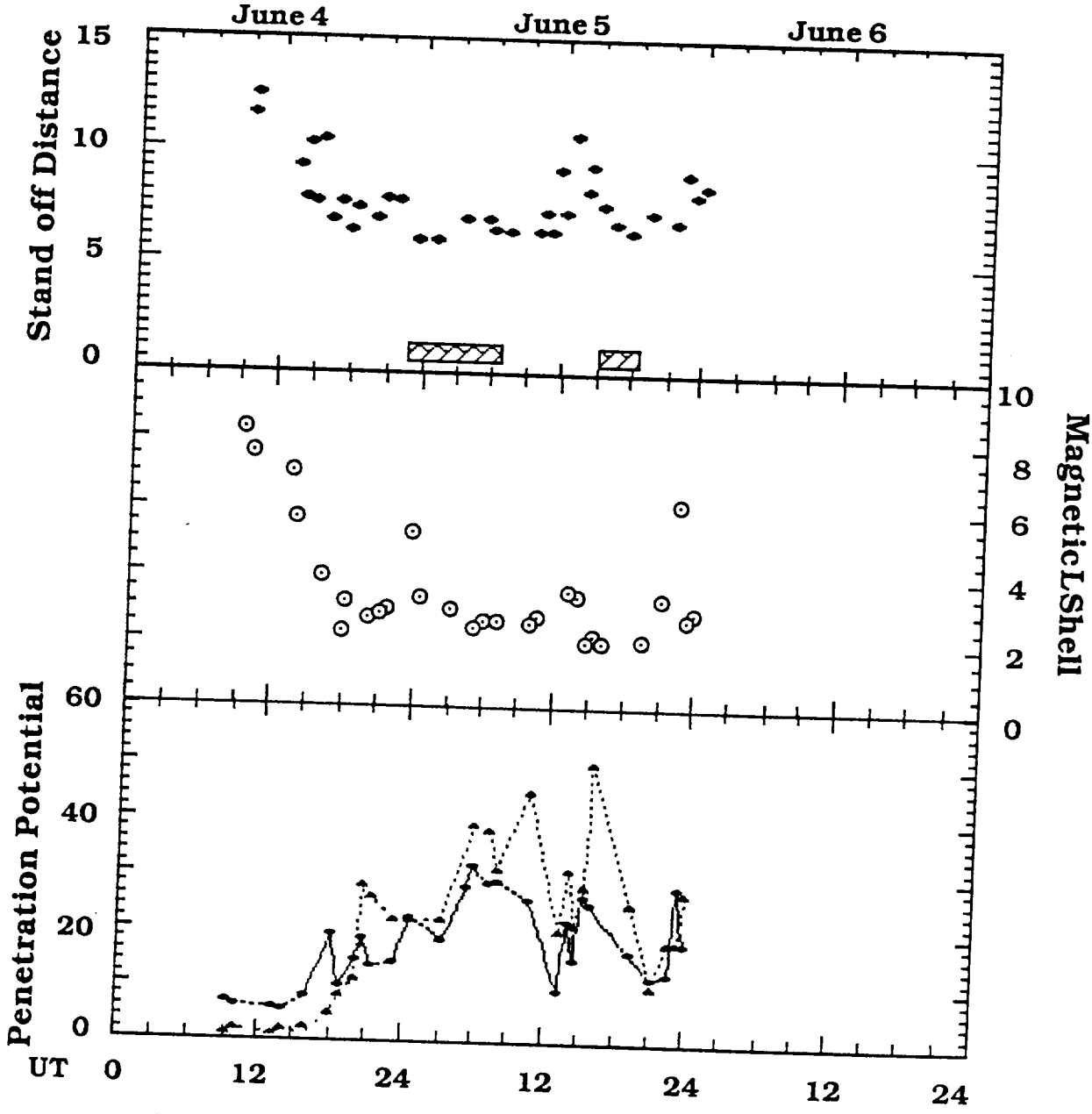

Figure 10. Comparison of observations with predictions of Volland–Stern model for June 4 - 5, 1991. The top plot gives the calculated values of L_{ss}. The middle plot contains predicted values of L_e using the magnetic local times at which DMSP F8 crossed the auroral electron boundary. The bottom plot shows predicted (diamonds) and measured (triangles) values of Φ_{pen}.

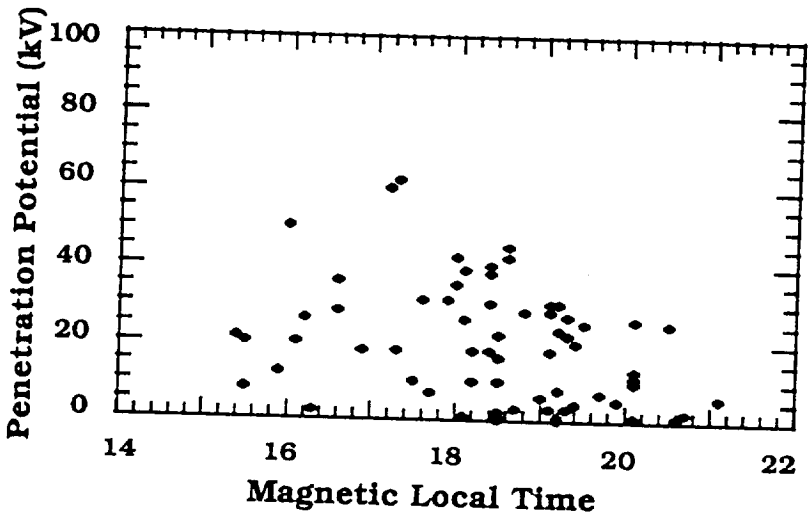

Figure 11. Scatter plot of measured Φ_{pen} versus magnetic local time on June 4 - 6, 1991.

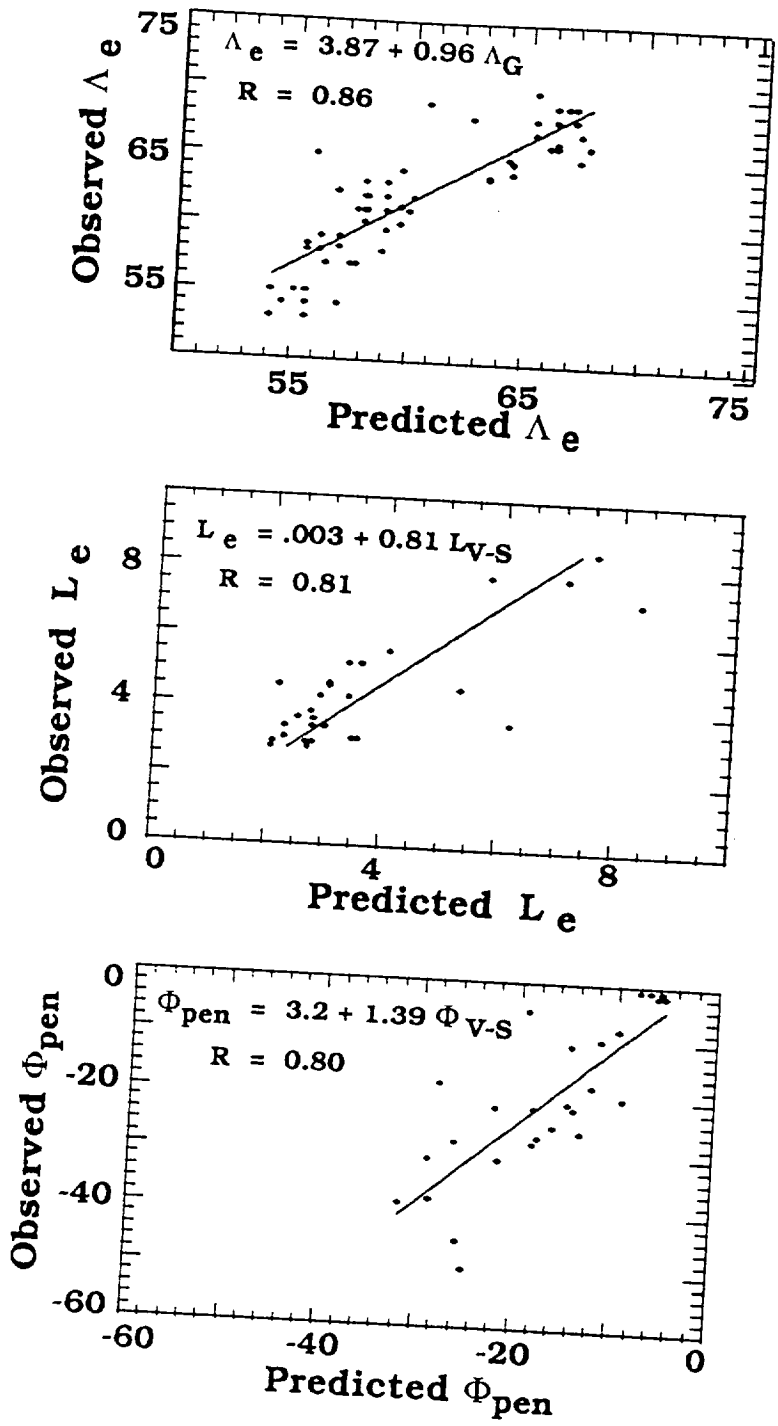

Figure 12. Scatter plots comparing observed values of Λ_e (top) and L_e (middle) with predictions of the empirical models of *Gussenhoven et al.* [1981] and Volland–Stern. The bottom plot compares measured with predicted values of Φ_{pen}.

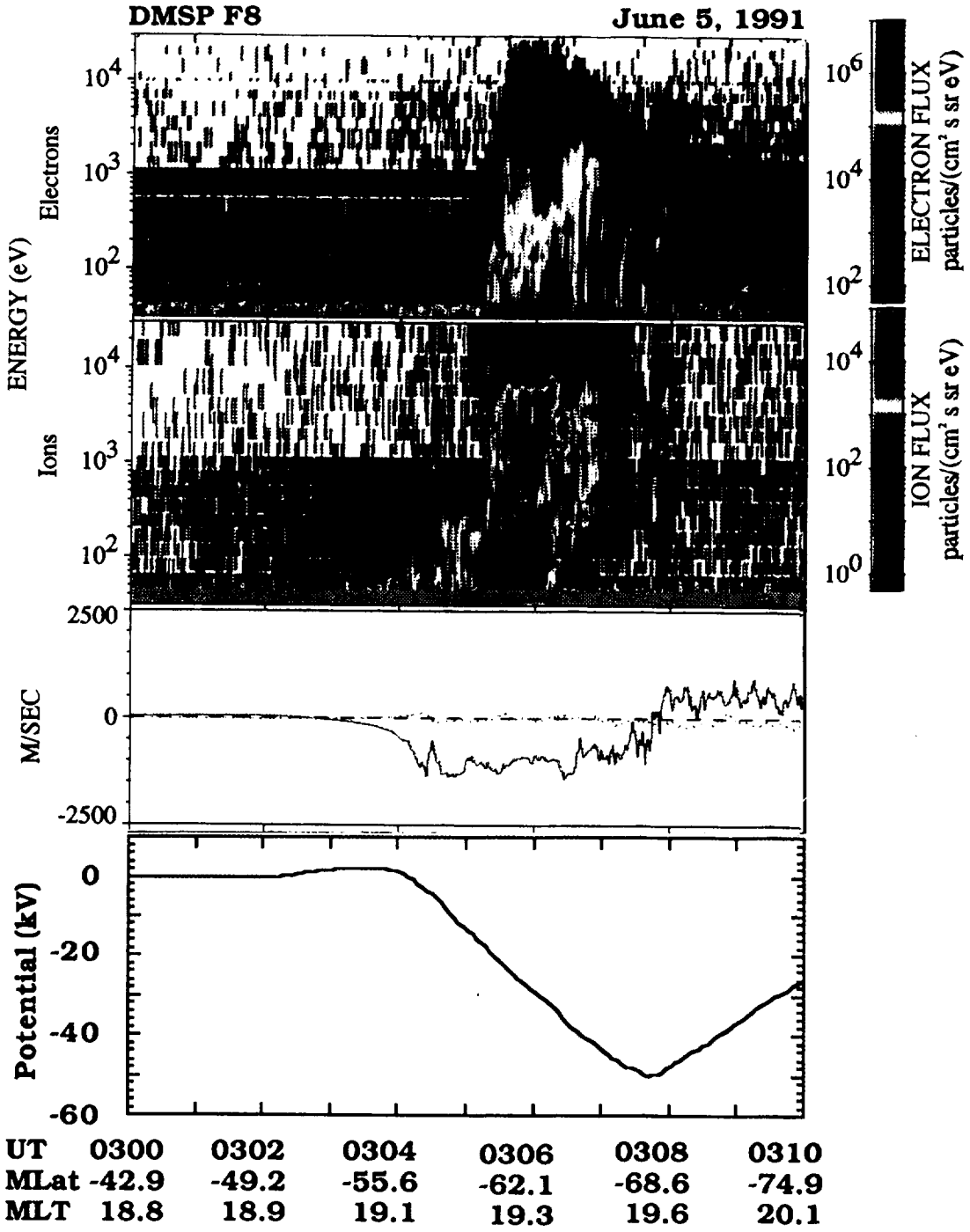

Plate 1. DMSP F8 measurements during the southern high latitude pass from 5/0300 to 0310 UT. The top two plots contain energy versus time spectrograms for downcoming electron and ion fluxes. Color codes for directional differential fluxes, particles (cm^2 s sr eV)$^{-1}$, are given to the right of the spectrograms. The third plot shows the horizontal (solid line) and vertical (dashed line) components of plasma drift. The bottom plot gives the potential distribution along the satellite trajectory.

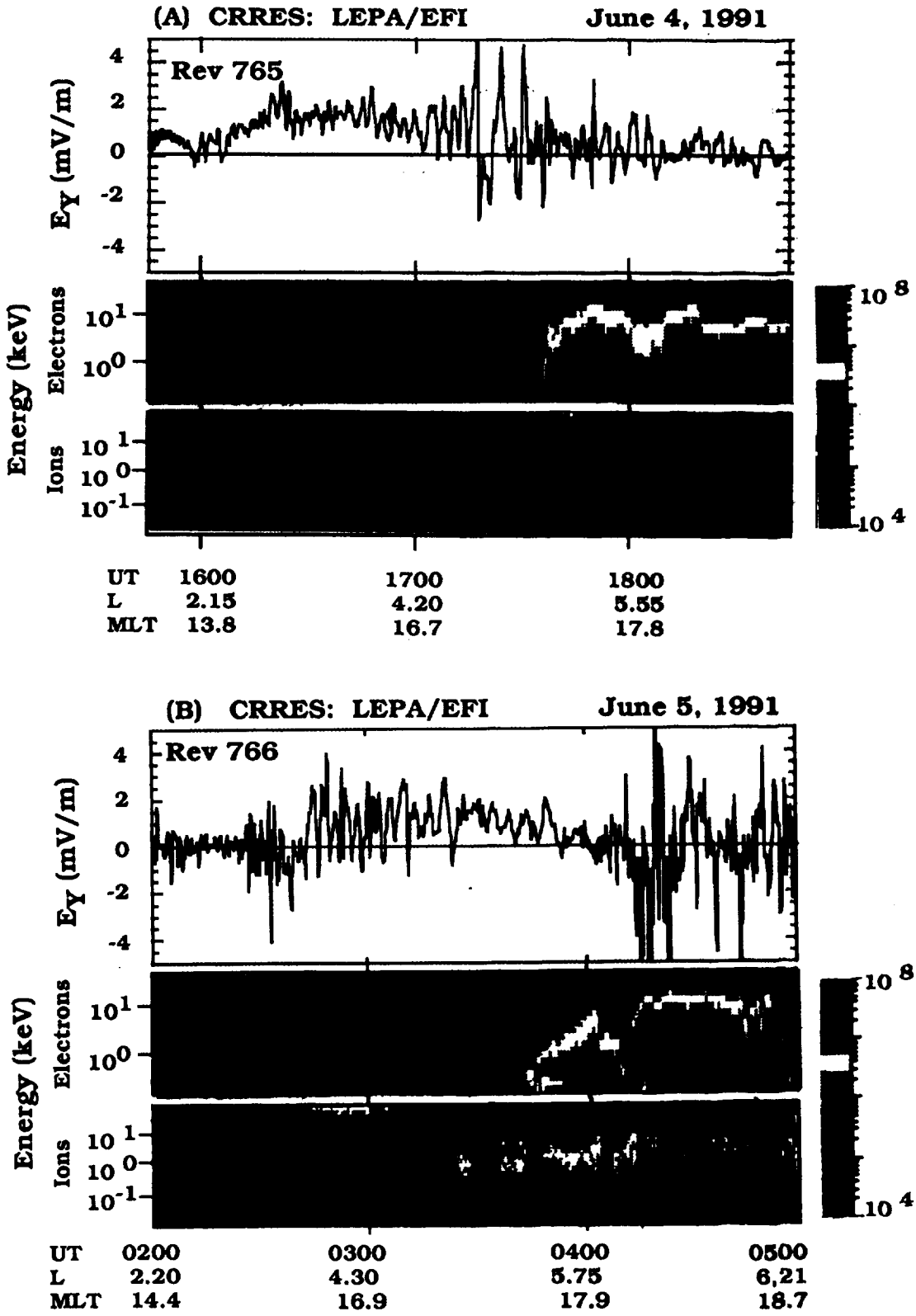

Plate 2. CRRES measurements of electric fields (top) and trapped particle fluxes during the outbound phase of orbits 765 (A) and 766 (B). The electric field component is positive approximately in the Y_{GSE} direction. The bottom two plots for each orbit contain energy versus time spectrograms for electrons and ions with pitch angles near 90°. Color codes for directional differential fluxes, particles $(cm^2\ s\ sr\ eV)^{-1}$, are given to the right of the spectrograms.